Fibroblast Stromal Support Model for Predicting Human Papillomavirus-Associated Cancer Drug Responses.

Claire D. James[a], Rachel L. Lewis[a], Alexis L. Fakunmoju[a], Austin J. Witt[a], Aya H. Youssef[a], Xu Wang[a], Nabiha M. Rais[a], Apurva Tadimari Prabhakar[a], J. Mathew Machado[a], Raymonde Otoa[a], Molly L. Bristol [a,b,#]

[a] Philips Institute for Oral Health Research, School of Dentistry, Virginia Commonwealth University (VCU), Richmond, Virginia, USA

[b] VCU Massey Comprehensive Cancer Center, Richmond, Virginia, USA

Running Title: Stroma Translational Model for HPV+ Cancer Responses

#Address correspondence to Molly L. Bristol, mlbristol@vcu.edu.

Abstract

Currently, there are no specific antiviral therapeutic approaches targeting Human papillomaviruses (HPVs), which cause around 5% of all human cancers. Specific antiviral reagents are particularly needed for HPV-related oropharyngeal cancers (HPV^+OPCs) whose incidence is increasing and for which there are no early diagnostic tools available. We and others have demonstrated that the estrogen receptor alpha (ERα) is overexpressed in HPV^+OPCs, compared to HPV-negative cancers in this region, and that these elevated levels are associated with an improved disease outcome. Utilizing this HPV^+ specific overexpression profile, we previously demonstrated that estrogen

attenuates the growth and cell viability of HPV^+ keratinocytes and HPV^+ cancer cells *in vitro*. Expansion of this work *in vivo* failed to replicate this sensitization. The role of stromal support from the tumor microenvironment (TME) has previously been tied to both the HPV lifecycle and *in vivo* therapeutic responses. Our investigations revealed that *in vitro* co-culture with fibroblasts attenuated HPV^+ specific estrogen growth responses. Continuing to monopolize on the HPV^+ specific overexpression of ERα, our co-culture models then assessed the suitability of the selective estrogen receptor modulators (SERMs), raloxifene and tamoxifen, and showed growth attenuation in a variety of our models to one or both of these drugs *in vitro.* Utilization of these SERMs *in vivo* closely resembled the sensitization predicted by our co-culture models. Therefore, the *in vitro* fibroblast co-culture model better predicts *in vivo* responses. We propose that utilization of our co-culture *in vitro* model can accelerate cancer therapeutic drug discovery.

Importance

Human papillomavirus-related cancers (HPV^+ cancers) remain a significant public health concern, and specific clinical approaches are desperately needed. In translating drug response data from *in vitro* to *in vivo*, the fibroblasts of the adjacent stromal support network play a key role. Our study presents the utilization of a fibroblast 2D co-culture system to better predict translational drug assessments for HPV^+ cancers. We also suggest that this co-culture system should be considered for other translational approaches. Predicting even a portion of treatment paradigms that may fail *in vivo* with a co-culture model will yield significant time, effort, resource, and cost efficiencies.

Keywords

Estrogen, ERα, stroma, HPV, human papillomavirus, oropharyngeal cancer, Raloxifene, Tamoxifen, therapeutics

Introduction

Human papillomaviruses (HPVs) are small, double-stranded DNA viruses, and high-risk HPVs are known carcinogens[1–7]. HPV is the most common sexually transmitted infection in the United States (U.S.), and estimated to infect more than 80% of the population at least once in their lifetime[1–3,8–12]. HPV16 is the most prevalent genotype, accounting for at least 50% of cervical cancers and approximately 90% of HPV^+ oropharyngeal cancers (HPV^+OPCs)[9,13,14]. While prophylactic HPV vaccines have already begun to show remarkable efficacy in preventing infection and related diseases, HPV continues to account for ~5% of worldwide cancer, and disproportionately affects marginalized populations both in the U.S. and around the world[1–3,8–12,15–17]. As such, the lack of specific antiviral therapeutics available for combatting HPV-related cancers is of significant concern.

While many cancers are on the decline, the last two decades have shown a sharp increase in HPV^+OPCs, for which there are no early diagnostic tools available[4–6,18,19]. HPV^+OPCs are found at 4-fold higher levels in men than in women, suggesting there are sex-related differences in the development of these cancers[4,18]. Using data from The Cancer Genome Atlas (TCGA), we and others have shown that the estrogen receptor alpha (ERα) is overexpressed in HPV^+HNC (head and neck cancers including OPCs) and that these elevated levels are associated with an improved disease outcome[18,20–26].

We have also previously demonstrated that 17-β estradiol (estrogen) attenuates the growth and cell viability of HPV^+ keratinocytes and HPV^+ cancer cells *in vitro,* but

not HPV negative (HPV^-) keratinocytes or HPV^- cancer cells[26]. Sensitization occurs via numerous mechanisms: 1) at the level of viral transcription, 2) via interactions with E6 and E7, 3) through manipulation of cell survival and cell death pathways[26]. Here, we report that the expansion of estrogen treatment into *in vivo NOD-scid IL2Rg*^{null} (NSG) mice revealed a lack of response to estrogen alone or in combination with radiotherapy (IR).

Previously, estrogen has been shown to promote HPV-induced cervical disease in immunocompetent mice, yet this enhancement was lost in NSGs[27–32]. HPV oncogenes, in conjunction with estrogen, were shown to fundamentally reprogram the tumor microenvironment (TME)[27,28,33]. We therefore sought to determine if the TME, specifically the stromal support provided by fibroblasts, alters the estrogenic effects in our model systems[33–42]. *In vitro* co-culture studies revealed that stromal interactions markedly change cell growth and viability in response to estrogen in our HPV^+ models.

While our estrogen studies did not prove effective *in vivo*, ERα remains overexpressed in HPV^+OPC and HPV^+ cervical cancers[24–27,29,31–33,43]. Selective estrogen receptor modulators (SERMs) have proven to provide a multitude of therapeutic applications[44–50]. Analysis of K14E6/E7 transgenic mice models have previously shown the possible utility of raloxifene on reduction of recurrence of cervical neoplastic disease, and earlier literature suggested the utility of tamoxifen to lengthen the latent period for cervical dysplasia and carcinoma in carcinogen-induced models[45,51]. We utilized our co-culture system to assess the efficacy of raloxifene and tamoxifen and showed significant growth repression to one or both SERMs in a number of cancer cell lines. Our preliminary assessment of these SERMs in an *in vivo* HPV^+HNC cell line correlated with

our *in vitro* observations and suggests that these drugs may be useful adjuvant approaches for further investigation. To our knowledge, our analysis is the first to provide evidence on the utility of SERMs for HPV^{+}OPCs.

Overall, this report further expands upon the analysis of utilizing estrogen related signaling in the quest for HPV-specific antiviral approaches[25]. While estrogen presented compelling evidence *in vitro*, this report demonstrates that estrogen treatment did not translate to *in vivo* models[26]. The development of co-culture models utilizing fibroblast "feeder" cells demonstrated that these supporting fibroblasts altered the response to estrogen *in vitro*, modeling what was observed *in vivo*. Analysis of SERMs with this co-culture model demonstrated the utility of altering estrogen-related signaling both *in vitro* and *in vivo*. Therefore, co-culture with fibroblasts offers a simple and more physiologically relevant environment by stimulating more of the cellular interactions present in solid tumors. This co-culture model may serve to better predict drug responses in other translational paradigms, not limited to HPV^{+} cancers. Co-culture allows for an examination of the complex cellular responses to drug effects *in vivo*, thereby enhancing the accuracy of *in vitro* therapeutic evaluations for more successful translational approaches.

Results

Estrogen sensitization is not observed *in vivo*

We have previously reported that estrogen attenuates the growth of epithelial cells in an HPV^{+} dependent manner *in vitro*[26]. We found that this occurred via both a repression of transcription from the HPV16 long control region and through interactions with the viral oncogenes, E6 and E7[26]. Furthermore, estrogen treatment enhanced

115 irradiation-induced cell death in an HPV$^+$ dependent manner[26]. A logical progression was
116 to assess the response of HPV$^+$ cancers to estrogen *in vivo*. Previously, our laboratory as
117 well as others have demonstrated that HeLa cells are highly responsive to estrogen
118 treatment[26,52,53]. Consequently, experiments were designed to assess the combination of
119 estrogen and radiation treatment on HeLa xenografts in female NSG mice. Contrary to
120 our *in vitro* data, Figure 1A shows that estrogen alone, or in combination with radiation,
121 had no impact on tumor response in mice. Of note, animal weights remained consistent
122 throughout the study with all treatments (Figure 1B).

123 Previously, we had observed HPV$^+$ dependent cell death following estrogen
124 treatment regardless of sex, tissue of origin, or viral genome integration status[26]. To
125 determine if any of these factors played a role *in vivo*, we decided to expand our analysis
126 to include the male, episomal, HPV16$^+$ oropharyngeal cancer cell line UMSCC104[54]. In
127 addition, we added "early" estrogen supplementation that began the same day as
128 xenografts were injected, to determine if a temporal relationship was essential to the
129 estrogen treatment response. As our previous radiation treatment using 10 Gy had some
130 off-target effects in our NSGs, radiation was reduced to 5 Gy in these studies. As
131 observed in Figure 1C (animal weight Figure 1D), estrogen again had no impact on tumor
132 response in any of these conditions. These results complement the previous observations
133 by the Lambert laboratory utilizing MmuPV1[27]. The Lambert observations demonstrated
134 that estrogenic effects *in vivo* are reliant, at least in part, on estrogen's suppression of the
135 host immune system in immunocompetent mice; whereas estrogenic enhancement of
136 disease progression were not observed in immunodeficient NSG mice[27]. Our results
137 indicate that the lack of estrogenic alterations in disease progression may not be

138 papillomavirus species specific, but further studies are needed to confirm this
139 observation.

140 **Stroma alters HPV-specific estrogen growth response in keratinocyte models**

141 There are numerous differences when moving from *in vitro* to *in vivo* models. An
142 increasingly recognized component of *in vivo* responses is the adjacent stromal support
143 network, or "tumor microenvironment" (TME)[33,55,56]. In regard to HPV, evidence also
144 supports a significant role for stroma during the viral lifecycle and HPV-induced disease
145 [33,39,41,42]. Fibroblasts are a key component of this stromal support and can significantly
146 alter cancer resistance and therapeutic responses[33–42]. We already utilize feeder layers of
147 mitomycin C (MMC) growth-arrested murine 3T3-J2 fibroblasts (referred to as J2s
148 moving forward) in the immortalization and maintenance of our primary keratinocyte
149 derived HPV^+ epithelial cultures. Thus, we applied the same approach to investigate
150 whether this co-culture system affects the response to estrogen. MMC inactivation is a
151 supported approach to arrest the proliferation of fibroblasts, allowing for the
152 establishment of a supportive feeder layer that maintains its ability to synthesize RNA
153 and protein and provide stromal regulation of neighboring cells of interest[57]. This
154 approach is widely accepted as necessary for maintenance of the HPV genome, as well as
155 a necessary component of 3D models for HPV lifecycle analysis[58–64]. N/Tert-1 cells
156 (telomerase immortalized foreskin keratinocytes, HPV negative), as well as HFK+E6E7
157 (foreskin keratinocytes immortalized by the viral oncogenes only), and HFK^+HPV16
158 (foreskin keratinocytes immortalized by the entire HPV16 genome, replicating as an
159 episome), were cultured in the presence or absence of J2 cells, and treated with 15μM
160 estrogen, or vehicle control[26]. Compared to untreated, non-cocultured N/Tert-1 cells, no

significant alterations in growth rate were observed following estrogen treatment or co-culture with J2s (Figure 2A). Conversely, estrogen significantly repressed the growth of both the E6E7 and HPV16 immortalized cell lines in the absence of stromal support (Figure 2B and 2C, respectively). The presence of stromal support fibroblasts significantly rescued this growth suppression (Figure 2B and 2C); coculture with fibroblasts mitigates the growth suppressive effects of estrogen, *in vitro*. This implies that the presence of stromal support is responsible for the differences in response to estrogen treatment that we observed between our *in vitro* and *in vivo* models (Figure 1)[26].

Stroma alters HPV-specific estrogen growth response in cancer models

We sought to expand our co-culture investigations to include cancer lines. A hallmark of transformation in many cancer cell lines is anchorage independent growth and loss of adherence in cell culture[65]. To improve our cancer cell count analysis, we developed a novel, quantifiable co-culture system. Using the Nuclight lentivirus system (Sartorius), we transduced our cells of interest with nuclear mKate2-red and developed stable cell lines; this system enabled automated cell counting and could distinguish between our cells of interest and the non-labeled J2s. An additional advantage of this system was the ability to monitor cellular morphology and observe any co-culture influences upon colony formation and cellular distribution. We sought to determine whether J2s alter cancer cell line responses to estrogen, as observed in our keratinocyte models (Figure 2). We utilized four cancer cell lines in our co-culture experiments: HN30 – an HPV^- head and neck cancer (p53wt), HeLa – an $HPV18^+$ integrated cervical cancer (p53wt), UMSCC47 – an $HPV16^+$ integrated head and neck cancer (p53wt), and UMSCC104 – an $HPV16^+$ episomal head and neck cancer (p53wt). As HeLa cells are

184 highly sensitive to estrogen, 1.5μM estrogen was utilized in experiments with these cells;
185 all other cell lines were treated with 15μM as previously described[26,52]. As previously
186 shown, estrogen treatment significantly repressed cell growth in an HPV^+ dependent
187 manner (Figures 3A,C,E,F)[26]. Conversely, estrogenic sensitivity was no longer observed
188 in HPV^+ cancer cells grown with feeder cells (Figures 3B,D,F,H). This was similar to the
189 loss of estrogenic sensitivity in our HPV^+ keratinocytes (Figure 2), and in our mouse
190 studies (Figure 1A, and 1C). Again, demonstrating that stromal support alters estrogenic
191 sensitivity of HPV^+ cancer models.

192 To determine if this repression of estrogenic sensitization was specific to mouse
193 fibroblast support in co-culture, HeLa cells were grown in the presence or absence of
194 conditioned media collected from replicating 3T3-J2s cultures, or grown in co-culture
195 with MMC-inactivated human dermal mesenchymal fibroblasts (HDFMs). Again Figure
196 4A demonstrates that HeLa cells in monoculture undergo significant growth repression in
197 the presence of estrogen. Similarly, estrogenic growth repression was observed in the
198 presence of J2 conditioned media (Figure 4B). Co-culture with HDFMs rescued
199 estrogenic growth repression in HeLa cells (Figure 4C), similar to what was observed
200 with J2s (Figure 3B). HDFMs did not repress the growth of HeLa alone (Figure 4C),
201 contrary to the growth repression observed in the presence with J2 (Figure 3B). While we
202 do not currently understand the mechanism behind this altered growth potential with
203 alternative species' fibroblasts, we find it noteworthy that estrogenic sensitivity is lost
204 with both co-culture methods, but not by incubation with media, indicating that cell-cell
205 contact is required. Moreover, this loss of sensitivity is not dependent on fibroblast
206 growth alteration of cancer cells.

Stroma does not alter the response to cisplatin in cancer models.

To assess the predictiveness of our co-culture model, we found it important to investigate whether stroma would alter the response to other chemotherapeutic approaches. HeLa, UMSCC47, UMSCC104, and HN30 cells were therefore evaluated for their responsiveness to cisplatin (Figure 5A,C,E,G). Fibroblasts did not rescue the growth arrest observed in all cell lines (Figures 5B,D,F,H). Cisplatin is a well-established clinical treatment paradigm for HPV^+ and HPV^-OPCs, cervical cancer, and many other cancers[66–74]. We predicted that fibroblasts would not be able to rescue cancer cells from this conventional chemotherapeutic agent. We postulate that fibroblasts are unlikely to change the response to most currently accepted cancer treatment modalities. Instead, we suggest that this model may better predict which novel therapeutics may fail translational approaches. This is something we are currently investigating, and we encourage others to consider this approach as well when translating treatments from *in vitro* to *in vivo*.

Stroma alters HPV long control region (LCR) transcriptional regulation

We previously published that estrogen represses transcription of the HPV16 long control region (LCR) both in our N/Tert-1 and C33a transcription models[26]. This transcriptional repression of the LCR, in turn, downregulated the expression of early viral genes in our numerous HPV^+ keratinocyte and HPV^+ cancer models[26]. Expanding upon these previous observations, we further wanted to determine the impact of stromal support on estrogenic HPV16-LCR transcriptional regulation. N/Tert-1 cells grown in the presence of stromal support had significantly enhanced levels of HPV16-LCR transcription and this transcriptional regulation was no longer significantly repressed by estrogen (Figure 6A); this may be one of the many contributing factors involved in the

loss of estrogen sensitivity. ERα was also assessed, and stroma did not appear to alter protein expression in N/Tert-1 cells (Figure 6B). These results suggest that stroma is highly supportive of HPV16-LCR transcriptional regulation.

Fibroblasts are routinely utilized to support HPV genome maintenance and the viral life cycle in keratinocyte models[33,41,57,75–82]. While this model is accepted, the full mechanism of how fibroblasts aid maintenance of the viral genome as an episome has yet to be elucidated. Figure 6A demonstrates that stromal support enhances HPV16-LCR transcription. It was therefore important to confirm that this transcriptional regulation had downstream effects. Previously, elements of the HPV upstream regulatory region, another term for the viral LCR, have been implicated as a requirement for long term viral persistence in keratinocytes[83]. The McBride laboratory demonstrated that the chromatin architecture of this region is important for genome partitioning and may influence integration[83]. Figure 6C confirms that HFK^{+}HPV16 begin to integrate the viral genome when grown in the absence of J2 for one week[84,85]. The accepted practice of fibroblast co-culture, may in part maintain viral episomes via influencing the transcription of LCR.

Thus, stroma supports viral protein expression and alters host signaling pathways in keratinocytes

We next investigated viral protein expression and host protein signaling observed in the presence or absence of fibroblast support. HFK+E6/E7, HFK^{+}HPV16, and N/Tert-1 cells (Figure 6D) were grown in the presence or absence of J2s. J2s are washed off before harvesting samples, and are murine-derived so there should be limited detection via human-specific antibodies. To confirm that altered protein levels observed were not due to any residual J2s, lane 1 in Figure 6D demonstrates that significant specific bands

were not observable with the majority of our chosen antibodies with 100µg of J2 protein input. SIRT1 does have a notable lower band which is not unexpected due to the gene homology between mouse and human SIRT1 and that the immunogen was developed from the amino acids 1-131 of mouse Sir2α. γH2AX has a low-level detectible band due to cross reactivity of the antibody; it should be noted that the significant observations discussed have taken this into account. Figure 6D demonstrates that HFK+E6E7, which do not rely on the LCR for early gene expression, do not have altered E7 protein levels in the presence or absence of fibroblasts (lanes 2,3). As fibroblasts were shown to enhance LCR transcription (Figure 6A), HFK^{+}HPV16 cells, which rely on the LCR for early gene expression, have enhanced E7 levels when grown in the presence of J2s (lanes 4,5). HFK+E6E7 had limited levels of p53 expression, and HFK^{+}HPV16 had low expression of p53, due to E6-targeted degradation; however significant enhancement of p53 levels in the presence of J2 in both cell lines were striking[63,64,79,86–91]. To our knowledge, this is the first report to suggest why p53 is not always fully degraded in HPV^{+} cell lines; E6 degradation of p53 may depend on whether or not keratinocytes are maintained on feeder cells[79,88,90,92–97]. Upregulation of p53 in the presence of J2 was also observed in N/Tert-1 cells (lanes 6,7) so this observation is independent from E6 or full genome expression. It is worth noting that HFK^{+}HPV16 cells are consistently maintained in co-culture with J2s, and that J2s were not supplemented for the "control" conditions. This also demonstrates that the stromal induced alterations of p53 protein levels are reversible (Figure 6D). Total levels of pRb were not altered N/Tert-1 cells nor in HFK+E6E7; this corresponds to unaltered E7 levels in HFK+E6E7 cells. Alternatively, pRb was reduced in HFK^{+}HPV16 grown in the presence of J2s. Again, suggesting fibroblasts are important for viral

regulation of keratinocyte signaling, possibly through the LCR. A consistent observation was the upregulation of γH2AX in the presence of J2s in all of the cell lines (Figure 6D). Numerous reports have demonstrated HPV viral integrity and genome stability is highly reliant on DNA repair machinery, including γH2AX; J2 enhancement of γH2AX may be another key mechanism of fibroblast regulation of viral genome stability in keratinocyte models[7,76,98–106]. Upstream of p53 and γH2AX, SIRT1 is known to target histones and non-histone substrates such as p53, and has been shown to decrease in response to DNA damage[107]. N/Tert-1 and HFK^{+}HPV16 grown in the presence of J2s demonstrated a significant decrease in SIRT1. The lower band observed can be associated with SIRT1 post-translational modifications; while this was altered by fibroblasts in both HFK+E6E7 and HFK^{+}HPV16, conclusions were not made due to the band observed with the J2 input sample [40,107–110]. While we are still investigating additional signaling mechanisms involved, these observations highlight the importance of properly controlling for whether or not cell lines are grown in the presence or absence of feeder cells when considering viral and host signaling events.

Selective estrogen receptor modulators reduce growth rates *in vitro* and *in vivo*

While estrogen had no impact on the tumor response in mice, alone or in combination with radiation (Figure 1), we expanded our analysis to assess if the selective estrogen receptor modulators (SERMs) raloxifene or tamoxifen would be a useful approach to continue to take advantage of the HPV^{+} specific overexpression of ERα. It should be noted that SERMs can be agonists or antagonists of the ERα, and these responses are dependent on region, cell type, and the localization and availability of estrogen response elements (EREs)[44,46,47,111]. Preclinical data supports the utility of

SERMs for cervical cancer, particularly the utility of raloxifene on the reduction of recurrent neoplastic disease; however, SERMs have yet to be evaluated in $HPV^{+}OPC$[47,111].

HeLa, UMSCC47, and UMSCC104 HPV^{+} cancer cells grown without fibroblast support exhibited significant growth repression to both SERMs (Figures 7A,C,E). While fibroblast support did not alter the response to SERMs in all the cell lines, rescued growth was observed in HeLa cells treated with tamoxifen while remaining responsive to raloxifene (Figures 7B,D,F). It is worth noting that previous *in vivo* and clinical analysis have predicted the utility of raloxifene in HPV^{+} cervical cancer response, whereas tamoxifen is not recommended[45–47,51,111]. We therefore sought to analyze SERM responsiveness in an $HPV^{+}HNC$ *in vivo* model. Expansion of SERM treatment *in vivo* was therefore conducted in UMSCC104 cells alone or in combination with IR to assess their utility as well as determine if our co-culture model could be useful in future translational approaches. For this study, 4 Gy IR was chosen to further reduce the off-target issues relating to radiation use in NSGs[112]. As observed in Figure 8A, radiation alone significantly reduced tumor volume starting on Day 14, while raloxifene (Figure 8A) and tamoxifen alone (Figure 8B) were able to significantly reduce tumor volume starting on Day 32. Furthermore, in comparison to radiation (IR) alone, tamoxifen+IR significantly reduced tumor volume starting on Day 42 (Figure 8B). Kaplan-Meier survival analysis demonstrated 50% survival for tamoxifen+IR on day 70 in comparison to 10% survival at the same time point for IR alone or raloxifene+IR at our chosen endpoint (Figure 8C). With all treatments, animal weights remained consistent throughout the study (Figure 8D). Our *in vitro* co-culture system modeled our *in vivo*

responses, as well as those previously observed, to both estrogen and SERMs in HPV$^+$ cervical *in vivo* models (Figure 1,3,7) [27,32,43,45–47,51,111]. Co-culture also predicted the responsiveness of SERMs in an HPV$^+$HNC *in vivo* model (Figure 7,8) and suggests that the utility of SERMs for the treatment of HPV$^+$OPC are worth further investigation. Altogether, we suggest that the predictiveness of this co-culture system should be considered in more translational approaches. Current studies are investigating the molecular mechanisms behind the alterations observed when cells are grown in fibroblast co-culture. These mechanistic approaches may further expand the predictive utility of our co-culture model.

Discussion

We previously established that estrogen attenuates the growth of HPV$^+$ keratinocyte and cancer cell lines in both an LCR and E6E7 dependent manner[25,26]. Of note, when these studies were conducted, we did not supplement fibroblast support during drug treatment[26]. Conversely, when estrogen was utilized to treat HPV$^+$ xenografts in NSG mice, responsiveness was no longer observed (Figure 1). This data is supportive of previous observations by the Lambert laboratory[27]. We acknowledge the importance of the immune system in the context of HPV, the responsiveness to estrogen, and its potential impact on translational approaches as well[27,28,45,113]. As NSG mice possess a significantly compromised immune system, we then sought to investigate the role that stromal support may play in the altered responsiveness to estrogen when moving from *in vitro* to *in vivo* models. In doing so, we found that there is an HPV-specific change in response to estrogen when comparing co-culture to non-fibroblast conditions (Figure 2,3,4). We find that this response is, at least in part, HPV16 LCR dependent; however,

there are likely other mechanisms at play (Figure 4). Additional mechanisms behind the observed stromal growth alterations, as well as the response to therapeutics, are currently under investigation in our laboratory and will be the subject of future reports.

Of note, the analysis of alternative species fibroblasts and mesenchymal cell types on basement membrane arrangement and growth characteristics of organotypic raft cultures were conducted many years ago[114]. Tissue-specific, species-specific, and spatial-specific alterations were found to impact numerous epithelial phenotypes[114]. Extracellular matrix components were found to have the greatest impact in this publication. We propose that the differences in extracellular matrix components between mouse and human might have moderate plating efficiency or growth efficiency alterations, and contribute to the altered growth potential observed in HeLa cells (Figure 3,4). As seen in Figure 3, UMSCC47 cell growth was not impacted by J2s; alternatively, UMSCC104 and HN30 cells grew better in the presence of J2. Regardless of the altered growth potential of cell lines in the presence or absence of fibroblasts, the observation that estrogenic sensitivity was lost in co-culture remains the same.

Anecdotally, is it known in the HPV field that J2s are crucial to the culture of primary keratinocytes for the maintenance of viral genome stability[75,76,104]. Expanding the accepted fibroblast co-culture system for HPV^{+} primary keratinocytes, our data demonstrates that this model promotes translational utility. When keratinocytes or cancer cells were grown in this co-culture system, *in vivo* results were more predictable. These models allowed for us to translate our estrogen results into estrogen pathway targeting drugs. Previous studies have highlighted the potential utility of SERMs in HPV^{+} cervical cancers, most specifically the use of raloxifene to reduce neoplastic recurrance[45,46,48,111].

We have expanded SERM analysis from cervical cancer to oropharyngeal cancer. We now demonstrate that SERMs may present clinical applicability as adjuvant approaches in HPV^{+}OPC and future investigations are warranted. While our observations apply both to primary keratinocytes and cancer models of HPV, we are currently in collaboration to expand analysis to other cancer treatment models. Nevertheless, stroma is recognized to contribute to the response to therapeutics and the development of resistance, and we conclude that it should be more often considered in future translational approaches[33,35,39,40,92].

Materials and Methods

Cell Culture

HN30 (generous gift from Hisashi Harada, VCU Philips Institute), UMSCC47 (Millipore; Burlington, MA, USA), and HeLa (generous gift from Alison McBride, NIAID) cells were grown in Dulbecco's modified Eagle's medium (DMEM) (Invitrogen; Carlsbad, CA, USA) supplemented with 10% charcoal/dextran stripped fetal bovine serum (Gemini Bio-products; West Sacramento, CA, USA). UMSCC104 (Millipore) cells were grown in Eagle's minimum essential medium (EMEM) (Invitrogen) supplemented with nonessential amino acids (NEAA) (Gibco) and 20% charcoal/dextran stripped fetal bovine serum. N/Tert-1 cells and all derived cell lines have been described previously and were maintained in keratinocyte-serum free medium (K-SFM; Invitrogen), supplemented with a 1% (vol/vol) PenStrep (Gibco) and previously described antibiotics[20–22,115–120]. HFK^{+}HPV16 have been previously described and were grown in Dermalife-K complete media (Lifeline Technology), and maintained on inactivated fibroblast feeder cells (described below)[121]. HFK+E6/E7 were grown in Dermalife-K

complete media (Lifeline Technology), and maintained on inactivated fibroblast feeder cells (described below); the immortalization process is described below. Of note, we have no issues with fibroblast plating efficiency, or keratinocyte viral episome maintenance utilizing these keratinocyte complete media kits over the traditional use of E-media[121,122]. For all cells not directly purchased from companies, the cell type was confirmed by Johns Hopkins or MD Anderson cell line authentication services, and the cells were maintained at 37°C in a 5% CO_2–95% air atmosphere, passaged every 3 or 4 days, and routinely monitored for mycoplasma (Sigma, MP0035).

Flank xenografts for *in vivo* drug trials

HeLa and UMSCC104 cells were stably transduced with a lentiviral vector for pLX304 Luciferase-V5 blast (generous gift from Renfeng Li, originally obtained from Kevin Janes, Addgene plasmid # 98580)[123]. Cell lines were selected with 10µg/ml blasticidin. Expression was verified with bioluminescent imaging, further outlined and defined in transcriptional activity analysis method detailed below.

Xenografting was performed using previously described methodology, in collaboration with the Virginia Commonwealth University (VCU) Cancer Mouse Models Core Laboratory (CMMC)[124,125]. All experiments were conducted in accordance with animal protocol AD10002330 approved by VCU Institutional Animal Care and Use Committee. NOD-SCID-IL2γ receptor null (NSG) mice (6-8 weeks old) were injected with $1x10^6$ cells suspended in PBS and Cultrex™ basement membrane extracts (BME) (Bio-techne/R&D Systems) into the right flank. HeLa studies were conducted in female mice; UMSCC104 studies were conducted in male mice (chosen to mimic sex from human donors). Days 1-3 post-xenograft and at varying times throughout the studies,

bioluminescence imaging was performed using a Xenogen IVIS-100 system (Calipers Life Sciences, Hopkinton, MA) to verify xenograft establishment, growth, and possible metastasis based on previously established protocols[126]. Tumor volume was also measured on noted dates and calculated as V =AB2 (π/6), where A is the longest dimension of the tumor, and B is the dimension of the tumor perpendicular to A. Data points presented on the graph are representative for each condition while more than 70% of the animals remained in each group. HeLa cells were palpable on day 10, UMSCC104 cells were palpable on day 7. It should be noted that in our hands, UMSCC104 xenografts are prone to ulceration. Animals were humanely euthanized when ulcerations were observed.

NSG estrogen delivery

A combinational approach for estrogen delivery was based on modified protocols designed in collaboration with the source of our obtained control and estrogen beeswax pellets (0.4mg estrogen, Huntsman Cancer Institute, University of Utah)[127,128]. Estrogen was also delivered in drinking water using a protocol kindly shared online by the Wicha lab[129]. Briefly, a 2.7 mg/mL stock of 17-estradiol (Sigma # E2758) in ethanol was diluted to a final concentration of 8 µg/mL in sterile drinking water. Pellets (control or estrogen) were implanted after tumors were palpable. Drinking water supplementation also began at this time point. “Early estrogen” in UMSCC104 denotes that water estrogen supplementation began the same day as xenograft injections (pellets were still implanted when tumors became palpable on day 7).

NSG SERM delivery

Treatment of mice with Raloxifene was performed as previously described by the Lambert Laboratory[45,111]. The human formulation of raloxifene hydrochloride (60mg tablets; EVISTA; Eli Lilly) were purchased from Virginia Commonwealth University Health System Pharmacy. Tablets were resuspended in PBS for a final concentration of 10 mg/ml. Mice were administered a 150 µl drug suspension (equivalent to 1.5 mg) via i.p. injection. Treatment of Tamoxifen was performed as previously described[130]. Tamoxifen (Sigma, T-5648) was resuspended in corn oil (Sigma C-8267) at 37°C for a final concentration of 10 mg/ml. Mice were administered 100 µl drug suspension (equivalent to 1.0 mg) via i.p. injection. SERM treatments began after tumors were palpable. Mice received treatment 5 days a week for 4 weeks, for a total of 20 injections.

Small Animal Radiation Research Platform (SARRP) ionizing radiation delivery

1 day following pellet implantation to allow for mouse recovery, targeted ionizing radiation (IR) was delivered utilizing the Xstrahal SARRP. HeLa studies utilized 10 Gy. Due to the radiation sensitivity of NSG mice, UMSCC104 studies reduced IR dose to 5 Gy, and finally to 4 Gy.

Culture, conditioned media collection, and mitomycin C (MMC) inactivation of 3T3-J2 mouse feeder cells

3T3-J2 immortalized mouse fibroblasts (J2) were grown in DMEM and supplemented with 10% FBS. Fresh media was exchanged twice a week; conditioned media was spun down as 500 rcf to remove any residual cells[131,132]. 80-90% confluent plates were supplemented with 4µg/ml of MMC in DMSO (Cell Signaling Technology) for 4-6 hours at 37°C. MMC-supplemented medium was removed and cells were washed with 1xPBS. Cells were trypsinized, spun down at 500 rcf for 5 mins, washed once with 1xPBS, spun

again, and resuspended. Quality control of inactivation (lack of proliferation) was monitored for each new batch of mitomycin-C. 100-mm plate conditions were supplemented with $1x10^6$ J2 and 6-well plate conditions were supplemented with $1x10^5$ every 2-3 days; for longer term cultures, any remaining J2s were washed off with 1x PBS and new J2 were continually supplemented every 2-3 days.

Culture and mitomycin C (MMC) inactivation of human dermal mesenchymal fibroblast feeder cells

Human dermal mesenchymal fibroblasts (HDFM) were grown, treated, and quality controlled as described for the above J2 protocol. 6-well plate conditions were supplemented with $1x10^5$ every 2-3 days.

Generation of E6E7-immortalized keratinocytes

Primary keratinocytes from single donors were obtained from LifeLine Cell Technologies[121]. Cells were cultured on collagen-coated plates for lentiviral delivery of HPV16 E6E7, using the pLXSN16E6E7 plasmid (Addgene plasmid # 52394, a gift from Denise Galloway)[133]. Following selection with G418 (72mM), cells were cultured on mitomycin-C inactivated 3T3-J2 fibroblasts. HFKs were cultured in DermaLife-K Complete media (LifeLine Cell Technologies) and E6E7 expression was confirmed by qRTPCR. Of note, these cells were generated at the same time and utilizing the same donors as the previously described HFK-HPV16[121].

Co-culture of keratinocytes in the presence or absence of inactivated fibroblasts

N/Tert-1, HFK E6E7, or HFK HPV16 cells were seeded at $5x10^5$ in 100-mm plates in the presence or absence of previously seeded J2s (at least 6 hours prior). Twenty-four hours later, noted cells were supplemented with 15 μM 17β-estradiol (estrogen). Forty-eight

hours after estrogen supplementation, plates were washed to remove residual J2 and cells were trypsinized and counted. For analysis of 1 week time point, HFK E6E7 or HFK HPV16 cells were seeded at $1x10^5$ in 100-mm plates in the presence or absence of previously seeded J2s. J2s were re-supplemented every 2-3 days as previously described. Pellets from these experiments were utilized for subsequent immunoblotting or DNA analysis, detailed below.

Generation of stable nuclear labeled cells with Incucyte® Nuclight Lentivirus

mKate2 Incucyte® Nuclight Lentivirus (puro) cells were generated according to the Sartorius product guide protocol (Sartorius cat# 4476), using a MOI of 3 or 6, depending on cell type. Cells generated were maintained in 1µg/ml puromycin supplemented media. Fluorescence was routinely monitored by BZ-X TexasRed filter via the Keyence BZ-X800 inverted fluorescence microscope.

Co-culture of nuclear-labeled cancer cell lines in the presence or absence of inactivated fibroblasts

Stable mKate2-puro HeLa, UMSCC47, UMSCC104, or HN30 cells were seeded in triplicate at $1x10^4$ per well in 6-well plates in the presence or absence of previously seeded J2 cells, or HDFM cells (at least 6 hours prior – fibroblast type is noted for each experiment). Twenty-four hours after seeding, day 0 images were captured in brightfield and TexasRed with the Keyence BZ-X800 Image Cytometer. Noted drugs were supplemented immediately after this initial imaging: 1.5µM (HeLa) or 15 µM 17β-estradiol (Sigma), 10µM Tamoxifen (MP Biomedicals), 10µM Raloxifene (Cayman Chemical Company), or 10-20µM Cisplatin (APExBIO). Cytometry images were again captured on day 1 and day 3. UMSCC104 were washed on day 3 after imaging, new J2

and drug were supplemented, and additional images were captured on day 5 and 7. Ten fields of view were randomized per well for all conditions. Cell count image cytometry batch analysis was performed using the Keyence BZ-X800 Image Analyzer software. All conditions utilized set analysis conditions from a single randomized control image and applied to all data points automatically to reduce variability and bias. Data is presented as fold of control from day 0. Representative images are presented in Figure 9.

Immunoblotting

Specified cells were washed with 1X PBS and trypsinized. Pellets were washed with 1X PBS and resuspended in 5X packed cell volume of NP40 buffer (50mM Tris-HCl Ph 7.5, 150mM NaCl, 1%NP-40, 5mM EDTA) supplemented with Roche cOmplete protease inhibitor and Roche PhosSTOP phosphatase inhibitor. Cell-lysis buffer suspension was incubated on ice for 30 min with occasional agitation, then centrifuged for 15 min at 14,000 rcf at 4 °C. Supernatant protein concentration was measured via the Bio-Rad protein estimation assay according to manufacturer's instructions. 100 µg protein samples were heated at 95 °C in 4x Laemmli sample buffer (Bio-Rad) for 5 min. Noted samples were run down a Novex 4–12% Tris-glycine gel (Invitrogen) and transferred onto a nitrocellulose membrane (Bio-Rad) at 30V overnight, or 100V for 1 hour using the wet-blot transfer method. Membranes were blocked with Odyssey (PBS) blocking buffer (diluted 1:1 with 1X PBS) at room temperature for 1 hour and probed with indicated primary antibody diluted in Odyssey blocking buffer. Membranes were washed with PBS supplemented with 0.1% Tween (PBS-Tween) and probed with the indicated Odyssey secondary antibody 1:10,000 (goat anti-mouse IRdye 800CW or goat anti-rabbit IRdye 680CW) diluted in Odyssey blocking buffer. Membranes were washed three times with

PBS-Tween and an additional wash with 1X PBS. Infrared imaging of the blot was performed using the Odyssey CLx Li-Cor imaging system. Immunoblots were quantified using ImageJ utilizing GAPDH as the internal loading control. The following primary antibodies were used for immunoblotting in this study at 1:1000, unless otherwise noted: ERα (Abcam, ab32063), GAPDH 1:10,000 (Santa Cruz, sc-47724), pRb (Santa Cruz, sc-102), p53 (Cell Signaling Technology, CST-2527 and CST-1C12), γH2AX 1:500 (Cell Signaling Technology, CST-80312 and CST-20E3), SIRT1 (EMD Millipore 07-131), β-actin (Santa Cruz, sc-47778), E7 1:500 (Santa Cruz, sc-6981).

Transfection and transcriptional activity analysis.

N/Tert-1 cells were plated at a density of 5×10^5 in 100-mm dishes. The following day, the previously described plasmids for pGL3 basic, pGL3 control, or pHPV16-LCR-Luc were transfected Lipofectamine 2000 (according to the manufacturer's instructions, ThermoFisher Scientific). Twenty-four hours after transfection, cells were washed, and noted cells were supplemented with 15 μM 17β-estradiol; J2s were also supplemented at this time point for noted conditions to reduce likelihood of altered transfection efficiency. Forty-eight hours after transfection, cells were harvested utilizing Promega reporter lysis buffer and analyzed for luciferase using the Promega luciferase assay system. Concentrations were normalized to protein levels, as measured by the Bio-Rad protein assay dye. Relative fluorescence units (RFU) were measured using the BioTek Synergy H1 hybrid reader.

Exonuclease V assay

PCR based analysis of viral genome status was performed using methods described by Myers *et al.* [84]. Briefly, 20 ng genomic DNA was either treated with exonuclease V

(RecBCD, NEB), in a total volume of 30 ul, or left untreated for 1 hour at 37°C followed by heat inactivation at 95°C for 10 minutes. 2 ng of digested/undigested DNA was then quantified by real time PCR using a 7500 FAST Applied Biosystems thermocycler with SYBR Green PCR Master Mix (Applied Biosystems) and 100 nM of primer in a 20 µl reaction. Nuclease free water was used in place of the template for a negative control. The following cycling conditions were used: 50°C for 2 minutes, 95°C for 10 minutes, 40 cycles at 95°C for 15 seconds, and a dissociation stage of 95°C for 15 seconds, 60°C for 1 minute, 95°C for 15 seconds, and 60°C for 15 seconds. Separate PCR reactions were performed to amplify HPV16 E6 F: 5'- TTGCTTTTCGGGATTTATGC-3' R: 5'-CAGGACACAGTGGCTTTTGA-3', HPV16 E2 F: 5'-TGGAAGTGCAGTTTGATGGA-3' R: 5'- CCGCATGAACTTCCCATACT-3', human mitochondrial DNA F: 5'-CAGGAGTAGGAGAGAGGGAGGTAAG-3' R: 5'-TACCCATCATAATCGGAGGCTTTGG -3', and human GAPDH DNA F: 5'-GGAGCGAGATCCCTCCAAAAT-3' R: 5'- GGCTGTTGTCATACTTCTCATGG-3'

Reproducibility, research integrity, and statistical analysis

All *in vitro* experiments were carried out at least in triplicate in all of the cell lines indicated. All cell lines were bought directly from sources indicated, or typed via cell line authentication services. All images shown are representatives from triplicate experiments. *In vivo* experiments were designed in collaboration with the VCU Massey Cancer Center animal core and biostats core for sample size justification and statistical power analysis. Quantification is presented as mean +/- standard error (SE). Student's t-test or analysis of variance (ANOVA) were used to determine significance as appropriate: * $p<0.05$, ** $p<0.01$, *** $p<0.001$

Data availability

Following the 2023 NIH data management and sharing policy, all data resulting from the development of projects will be available in scientific communications presented at conferences and in manuscripts that will be published in peer-reviewed scientific journals. Data will be deposited in the Open Science Framework (OSF) platform. OSF can be accessed at https://osf.io. VCU is an OSF institutional member, and OSF is an approved generalist repository for the 2023 NIH data management and sharing policy.

Acknowledgements

This work was supported by the VCU Philips Institute for Oral Health Research, the National Institute of Dental and Craniofacial Research/NIH/DHHS R03 DE029548, and the National Cancer Institute-designated Massey Cancer Center grant P30 CA016059. Mouse services and products in support of the research project were generated by the Virginia Commonwealth University Cancer Mouse Models Core Laboratory, supported, in part, with funding from NIH-NCI Cancer Center Support Grant P30 CA016059.

References

1. Brianti, P., De Flammineis, E. & Mercuri, S. R. Review of HPV-related diseases and cancers. *New Microbiol.* **40**, 80–85 (2017).
2. de Martel, C., Plummer, M., Vignat, J. & Franceschi, S. Worldwide burden of cancer attributable to HPV by site, country and HPV type. *Int. J. Cancer* **141**, 664–670 (2017).
3. McBride, A. A. & Münger, K. Expert Views on HPV Infection. *Viruses* **10**, 94 (2018).

4. Marur, S., D'Souza, G., Westra, W. H. & Forastiere, A. A. HPV-associated head and neck cancer: a virus-related cancer epidemic. *Lancet Oncol.* **11**, 781–789 (2010).

5. Lowy, D. R. & Munger, K. Prognostic implications of HPV in oropharyngeal cancer. *N. Engl. J. Med.* **363**, 82–84 (2010).

6. Sheedy, T. & Heaton, C. HPV-associated oropharyngeal cancer. *Jaapa* **32**, 26–31 (2019).

7. Porter, V. L. & Marra, M. A. The Drivers, Mechanisms, and Consequences of Genome Instability in HPV-Driven Cancers. *Cancers* **14**, 4623 (2022).

8. Chesson, H. W., Dunne, E. F., Hariri, S. & Markowitz, L. E. The estimated lifetime probability of acquiring human papillomavirus in the United States. *Sex. Transm. Dis.* **41**, 660–664 (2014).

9. Kang, S. D. *et al.* Effect of Productive Human Papillomavirus 16 Infection on Global Gene Expression in Cervical Epithelium. *J. Virol.* **92**, e01261-18 (2018).

10. McLaughlin-Drubin, M. E. & Meyers, C. Evidence for the coexistence of two genital HPV types within the same host cell in vitro. *Virology* **321**, 173–180 (2004).

11. McLaughlin-Drubin, M. E. & Münger, K. Oncogenic activities of human papillomaviruses. *Virus Res.* **143**, 195–208 (2009).

12. McLaughlin-Drubin, M. E., Meyers, J. & Munger, K. Cancer associated human papillomaviruses. *Curr. Opin. Virol.* **2**, 459–466 (2012).

13. zur Hausen, H. Papillomaviruses in the causation of human cancers - a brief historical account. *Virology* **384**, 260–265 (2009).

14. Psyrri, A. & DiMaio, D. Human papillomavirus in cervical and head-and-neck cancer. *Nat. Clin. Pract. Oncol.* **5**, 24–31 (2008).

15. Huh, W. K. *et al.* Final efficacy, immunogenicity, and safety analyses of a nine-valent human papillomavirus vaccine in women aged 16–26 years: a randomised, double-blind trial. *The Lancet* **390**, 2143–2159 (2017).

16. Kavanagh, K. *et al.* Changes in the prevalence of human papillomavirus following a national bivalent human papillomavirus vaccination programme in Scotland: a 7-year cross-sectional study. *Lancet Infect. Dis.* **17**, 1293–1302 (2017).

17. Meeting, I. W. G. on the E. of C. R. to H. & Cancer, I. A. for R. on. *Human Papillomaviruses*. (World Health Organization, 2007).

18. Sung, H. *et al.* Global Cancer Statistics 2020: GLOBOCAN Estimates of Incidence and Mortality Worldwide for 36 Cancers in 185 Countries. *CA. Cancer J. Clin.* **71**, 209–249 (2021).

19. Roman, B. R. & Aragones, A. Epidemiology and incidence of HPV-related cancers of the head and neck. *J. Surg. Oncol.* **124**, 920–922 (2021).

20. Nulton, T. J., Olex, A. L., Dozmorov, M., Morgan, I. M. & Windle, B. Analysis of The Cancer Genome Atlas sequencing data reveals novel properties of the human papillomavirus 16 genome in head and neck squamous cell carcinoma. *Oncotarget* **8**, 17684–17699 (2017).

21. Evans, M. R. *et al.* An oral keratinocyte life cycle model identifies novel host genome regulation by human papillomavirus 16 relevant to HPV positive head and neck cancer. *Oncotarget* **8**, 81892–81909 (2017).

22. Evans, M. R. *et al.* Human Papillomavirus 16 E2 Regulates Keratinocyte Gene Expression Relevant to Cancer and the Viral Life Cycle. *J. Virol.* **93**, e01941-18 (2019).

23. Nulton, T. J., Kim, N.-K., DiNardo, L. J., Morgan, I. M. & Windle, B. Patients with integrated HPV16 in head and neck cancer show poor survival. *Oral Oncol.* **80**, 52–55 (2018).

24. Kano, M. *et al.* Expression of estrogen receptor alpha is associated with pathogenesis and prognosis of human papillomavirus-positive oropharyngeal cancer. *Int. J. Cancer* **145**, 1547–1557 (2019).

25. James, C. D., Morgan, I. M. & Bristol, M. L. The Relationship between Estrogen-Related Signaling and Human Papillomavirus Positive Cancers. *Pathog. Basel Switz.* **9**, 403 (2020).

26. Bristol, M. L., James, C. D., Wang, X., Fontan, C. T. & Morgan, I. M. Estrogen Attenuates the Growth of Human Papillomavirus-Positive Epithelial Cells. *mSphere* **5**, e00049-20 (2020).

27. Wang, W. *et al.* Stress keratin 17 and estrogen support viral persistence and modulate the immune environment during cervicovaginal murine papillomavirus infection. *Proc. Natl. Acad. Sci. U. S. A.* **120**, e2214225120 (2023).

28. Spurgeon, M. E. *et al.* Human papillomavirus oncogenes reprogram the cervical cancer microenvironment independently of and synergistically with estrogen. *Proc. Natl. Acad. Sci. U. S. A.* **114**, E9076–E9085 (2017).

29. Chung, S.-H., Wiedmeyer, K., Shai, A., Korach, K. S. & Lambert, P. F. Requirement for estrogen receptor alpha in a mouse model for human papillomavirus-associated cervical cancer. *Cancer Res.* **68**, 9928–9934 (2008).

30. Jabbar, S. F., Abrams, L., Glick, A. & Lambert, P. F. Persistence of high-grade cervical dysplasia and cervical cancer requires the continuous expression of the human papillomavirus type 16 E7 oncogene. *Cancer Res.* **69**, 4407–4414 (2009).

31. Son, J., Park, J. W., Lambert, P. F. & Chung, S.-H. Requirement of estrogen receptor alpha DNA-binding domain for HPV oncogene-induced cervical carcinogenesis in mice. *Carcinogenesis* **35**, 489–496 (2014).

32. Chung, S.-H., Franceschi, S. & Lambert, P. F. Estrogen and ERalpha: culprits in cervical cancer? *Trends Endocrinol. Metab. TEM* **21**, 504–511 (2010).

33. Spurgeon, M. E. & Lambert, P. F. Human Papillomavirus and the Stroma: Bidirectional Crosstalk during the Virus Life Cycle and Carcinogenesis. *Viruses* **9**, 219 (2017).

34. Jensen, C. & Teng, Y. Is It Time to Start Transitioning From 2D to 3D Cell Culture? *Front. Mol. Biosci.* **7**, (2020).

35. Alkasalias, T., Moyano-Galceran, L., Arsenian-Henriksson, M. & Lehti, K. Fibroblasts in the Tumor Microenvironment: Shield or Spear? *Int. J. Mol. Sci.* **19**, 1532 (2018).

36. Truffi, M., Sorrentino, L. & Corsi, F. Fibroblasts in the Tumor Microenvironment. *Adv. Exp. Med. Biol.* **1234**, 15–29 (2020).

682 37. Monteran, L. & Erez, N. The Dark Side of Fibroblasts: Cancer-Associated
683 Fibroblasts as Mediators of Immunosuppression in the Tumor Microenvironment.
684 *Front. Immunol.* **10**, (2019).
685 38. Mao, X. *et al.* Crosstalk between cancer-associated fibroblasts and immune cells in
686 the tumor microenvironment: new findings and future perspectives. *Mol. Cancer* **20**,
687 131 (2021).
688 39. De Nola, R., Loizzi, V., Cicinelli, E. & Cormio, G. Dynamic crosstalk within the
689 tumor microenvironment of uterine cervical carcinoma: baseline network, iatrogenic
690 alterations, and translational implications. *Crit. Rev. Oncol. Hematol.* **162**, 103343
691 (2021).
692 40. Han, L. *et al.* Senescent Stromal Cells Promote Cancer Resistance through SIRT1
693 Loss-Potentiated Overproduction of Small Extracellular Vesicles. *Cancer Res.* **80**,
694 3383–3398 (2020).
695 41. Barros, M. R. *et al.* Activities of stromal and immune cells in HPV-related cancers.
696 *J. Exp. Clin. Cancer Res.* **37**, 137 (2018).
697 42. Raikhy, G. *et al.* Suppression of Stromal Interferon Signaling by Human
698 Papillomavirus 16. *J. Virol.* **93**, 10.1128/jvi.00458-19 (2019).
699 43. Chung, S.-H., Shin, M. K., Korach, K. S. & Lambert, P. F. Requirement for Stromal
700 Estrogen Receptor Alpha in Cervical Neoplasia. *Horm. Cancer* **4**, 50–59 (2013).
701 44. Martinkovich, S., Shah, D., Planey, S. L. & Arnott, J. A. Selective estrogen receptor
702 modulators: tissue specificity and clinical utility. *Clin. Interv. Aging* **9**, 1437–1452
703 (2014).

45. Spurgeon, M. E., Chung, S.-H. & Lambert, P. F. Recurrence of cervical cancer in mice after selective estrogen receptor modulator therapy. *Am. J. Pathol.* **184**, 530–540 (2014).

46. Munger, K. Are selective estrogen receptor modulators (SERMs) a therapeutic option for HPV-associated cervical lesions and cancers? *Am. J. Pathol.* **184**, 358–361 (2014).

47. Castle, P. E. Do Selective Estrogen Receptor Modulators Treat Cervical Precancer and Cancer? Time to Pool Data from Relevant Trials. *Int. J. Cancer J. Int. Cancer* **128**, 997–998 (2011).

48. Patel, H. K. & Bihani, T. Selective estrogen receptor modulators (SERMs) and selective estrogen receptor degraders (SERDs) in cancer treatment. *Pharmacol. Ther.* **186**, 1–24 (2018).

49. Johnston, S. R. Endocrine manipulation in advanced breast cancer: recent advances with SERM therapies. *Clin. Cancer Res. Off. J. Am. Assoc. Cancer Res.* **7**, 4376s–4387s; discussion 4411s-4412s (2001).

50. Moshi, M. R. *et al.* The Clinical Effectiveness of Denosumab (Prolia®) for the Treatment of Osteoporosis in Postmenopausal Women, Compared to Bisphosphonates, Selective Estrogen Receptor Modulators (SERM), and Placebo: A Systematic Review and Network Meta-Analysis. *Calcif. Tissue Int.* **112**, 631–646 (2023).

51. Sengupta, A., Dutta, S. & Mallick, R. Modulation of Cervical Carcinogenesis by Tamoxifen in a Mouse Model System. *Oncology* **48**, 258–261 (2009).

52. Li, D. *et al.* Estrogen-Related Hormones Induce Apoptosis by Stabilizing Schlafen-12 Protein Turnover. *Mol. Cell* **75**, 1103-1116.e9 (2019).

53. Liu, Y., Tian, L.-B., Yang, H.-Y. & Zhang, H.-P. Effects of estradiol and progesterone on the growth of HeLa cervical cancer cells. *Eur. Rev. Med. Pharmacol. Sci.* **21**, 3959–3965 (2017).

54. Tang, A. L. *et al.* UM-SCC-104: a new human papillomavirus-16 containing head and neck squamous cell carcinoma cell line. *Head Neck* **34**, 1480–1491 (2012).

55. Bożyk, A., Wojas-Krawczyk, K., Krawczyk, P. & Milanowski, J. Tumor Microenvironment—A Short Review of Cellular and Interaction Diversity. *Biology* **11**, 929 (2022).

56. Jin, M.-Z. & Jin, W.-L. The updated landscape of tumor microenvironment and drug repurposing. *Signal Transduct. Target. Ther.* **5**, 1–16 (2020).

57. Doorbar, J. *et al.* The biology and life-cycle of human papillomaviruses. *Vaccine* **30 Suppl 5**, F55-70 (2012).

58. Psyrri, A. & DiMaio, D. Human papillomavirus in cervical and head-and-neck cancer. *Nat. Clin. Pract. Oncol.* **5**, 24–31 (2008).

59. Huh, W. K. *et al.* Final efficacy, immunogenicity, and safety analyses of a nine-valent human papillomavirus vaccine in women aged 16–26 years: a randomised, double-blind trial. *The Lancet* **390**, 2143–2159 (2017).

60. Kavanagh, K. *et al.* Changes in the prevalence of human papillomavirus following a national bivalent human papillomavirus vaccination programme in Scotland: a 7-year cross-sectional study. *Lancet Infect. Dis.* **17**, 1293–1302 (2017).

748 61. Meeting, I. W. G. on the E. of C. R. to H. & Cancer, I. A. for R. on. *Human*
749 *Papillomaviruses*. (World Health Organization, 2007).
750 62. Vats, A., Trejo-Cerro, O., Thomas, M. & Banks, L. Human papillomavirus E6 and
751 E7: What remains? *Tumour Virus Res.* **11**, 200213 (2021).
752 63. The Expression of HPV E6/E7 mRNA In Situ Hybridization in HP... : International
753 Journal of Gynecological Pathology.
754 https://journals.lww.com/intjgynpathology/Fulltext/2023/01000/The_Expression_of
755 _HPV_E6_E7_mRNA_In_Situ.2.aspx.
756 64. Basukala, O. & Banks, L. The Not-So-Good, the Bad and the Ugly: HPV E5, E6
757 and E7 Oncoproteins in the Orchestration of Carcinogenesis. *Viruses* **13**, 1892
758 (2021).
759 65. Comprehensive understanding of anchorage-independent survival and its
760 implication in cancer metastasis | Cell Death & Disease.
761 https://www.nature.com/articles/s41419-021-03890-7.
762 66. Kiyota, N. *et al.* Weekly Cisplatin Plus Radiation for Postoperative Head and Neck
763 Cancer (JCOG1008): A Multicenter, Noninferiority, Phase II/III Randomized
764 Controlled Trial. *J. Clin. Oncol.* **40**, 1980 (2022).
765 67. Helfenstein, S. *et al.* 3-weekly or weekly cisplatin concurrently with radiotherapy
766 for patients with squamous cell carcinoma of the head and neck – a multicentre,
767 retrospective analysis. *Radiat. Oncol.* **14**, 32 (2019).
768 68. Cheng, Y., Li, S., Gao, L., Zhi, K. & Ren, W. The Molecular Basis and Therapeutic
769 Aspects of Cisplatin Resistance in Oral Squamous Cell Carcinoma. *Front. Oncol.*
770 **11**, 761379 (2021).

771 69. Rades, D. *et al.* Chemoradiation with Cisplatin vs. Carboplatin for Squamous Cell
772 Carcinoma of the Head and Neck (SCCHN). *Cancers* **15**, 3278 (2023).
773 70. Gold, J. M. & Raja, A. Cisplatin. in *StatPearls* (StatPearls Publishing, Treasure
774 Island (FL), 2024).
775 71. Ozols, R. F. *et al.* Phase III trial of carboplatin and paclitaxel compared with
776 cisplatin and paclitaxel in patients with optimally resected stage III ovarian cancer: a
777 Gynecologic Oncology Group study. *J. Clin. Oncol. Off. J. Am. Soc. Clin. Oncol.*
778 **21**, 3194–3200 (2003).
779 72. Kondagunta, G. V. *et al.* Combination of paclitaxel, ifosfamide, and cisplatin is an
780 effective second-line therapy for patients with relapsed testicular germ cell tumors.
781 *J. Clin. Oncol. Off. J. Am. Soc. Clin. Oncol.* **23**, 6549–6555 (2005).
782 73. Wang, H. *et al.* Cisplatin prevents breast cancer metastasis through blocking early
783 EMT and retards cancer growth together with paclitaxel. *Theranostics* **11**, 2442–
784 2459 (2021).
785 74. Nguyen, V. T. *et al.* Dose-Intense Cisplatin-Based Neoadjuvant Chemotherapy
786 Increases Survival in Advanced Cervical Cancer: An Up-to-Date Meta-Analysis.
787 *Cancers* **14**, 842 (2022).
788 75. Chapman, S., Liu, X., Meyers, C., Schlegel, R. & McBride, A. A. Human
789 keratinocytes are efficiently immortalized by a Rho kinase inhibitor. *J. Clin. Invest.*
790 **120**, 2619–2626 (2010).
791 76. Warburton, A., Markowitz, T. E., Katz, J. P., Pipas, J. M. & McBride, A. A.
792 Recurrent integration of human papillomavirus genomes at transcriptional
793 regulatory hubs. *NPJ Genomic Med.* **6**, 101 (2021).

77. Meyers, C. Organotypic (raft) epithelial tissue culture system for the differentiation-dependent replication of papillomavirus. *Methods Cell Sci.* **18**, 201–210 (1996).

78. Lambert, P. F. *et al.* Using an immortalized cell line to study the HPV life cycle in organotypic 'raft' cultures. *Methods Mol. Med.* **119**, 141–155 (2005).

79. Bienkowska-Haba, M. *et al.* A new cell culture model to genetically dissect the complete human papillomavirus life cycle. *PLOS Pathog.* **14**, e1006846 (2018).

80. Roberts, S., Evans, D., Mehanna, H. & Parish, J. L. Modelling human papillomavirus biology in oropharyngeal keratinocytes. *Philos. Trans. R. Soc. Lond. B. Biol. Sci.* **374**, 20180289 (2019).

81. Stanley, M. A., Pett, M. R. & Coleman, N. HPV: from infection to cancer. *Biochem. Soc. Trans.* **35**, 1456–1460 (2007).

82. Warburton, A., Della Fera, A. N. & McBride, A. A. Dangerous Liaisons: Long-Term Replication with an Extrachromosomal HPV Genome. *Viruses* **13**, 1846 (2021).

83. Coursey, T. L., Van Doorslaer, K. & McBride, A. A. Regulation of Human Papillomavirus 18 Genome Replication, Establishment, and Persistence by Sequences in the Viral Upstream Regulatory Region. *J. Virol.* **95**, e0068621 (2021).

84. Myers, J. E., Zwolinska, K., Sapp, M. J. & Scott, R. S. An Exonuclease V–qPCR Assay to Analyze the State of the Human Papillomavirus 16 Genome in Cell Lines and Tissues. *Curr. Protoc. Microbiol.* **59**, e119 (2020).

85. James, C. D. *et al.* HPV16 genome structure analysis in oropharyngeal cancer PDXs identifies tumors with integrated and episomal genomes. *Press* (2024).

86. Thomas, M., Pim, D. & Banks, L. The role of the E6-p53 interaction in the molecular pathogenesis of HPV. *Oncogene* **18**, 7690–7700 (1999).

87. Li, S. *et al.* Ubiquitination of the HPV Oncoprotein E6 Is Critical for E6/E6AP-Mediated p53 Degradation. *Front. Microbiol.* **10**, (2019).

88. Scheffner, M., Huibregtse, J. M., Vierstra, R. D. & Howley, P. M. The HPV-16 E6 and E6-AP complex functions as a ubiquitin-protein ligase in the ubiquitination of p53. *Cell* **75**, 495–505 (1993).

89. Graham, S. V. Keratinocyte Differentiation-Dependent Human Papillomavirus Gene Regulation. *Viruses* **9**, 245 (2017).

90. Huibregtse, J. M., Scheffner, M. & Howley, P. M. A cellular protein mediates association of p53 with the E6 oncoprotein of human papillomavirus types 16 or 18. *EMBO J.* **10**, 4129–4135 (1991).

91. Hoppe-Seyler, K., Bossler, F., Braun, J. A., Herrmann, A. L. & Hoppe-Seyler, F. The HPV E6/E7 Oncogenes: Key Factors for Viral Carcinogenesis and Therapeutic Targets. *Trends Microbiol.* **26**, 158–168 (2018).

92. Sahebali, S. *et al.* Stromal issues in cervical cancer: a review of the role and function of basement membrane, stroma, immune response and angiogenesis in cervical cancer development. *Eur. J. Cancer Prev.* **19**, 204–215 (2010).

93. Deng, H., Hillpot, E., Mondal, S., Khurana, K. K. & Woodworth, C. D. HPV16-Immortalized Cells from Human Transformation Zone and Endocervix are More Dysplastic than Ectocervical Cells in Organotypic Culture. *Sci. Rep.* **8**, 15402 (2018).

838 94. Dakic, A. *et al.* ROCK inhibitor reduces Myc-induced apoptosis and mediates
839 immortalization of human keratinocytes. *Oncotarget* **7**, 66740–66753 (2016).
840 95. Epithelial–Stromal Interactions Modulating Penetration of Matrigel Membranes by
841 HPV 16-Immortalized Keratinocytes. *J. Invest. Dermatol.* **109**, 619–625 (1997).
842 96. Waggoner, S. E. *et al.* Human Cervical Cells Immortalized in Vitro with Oncogenic
843 Human Papillomavirus DNA Differentiate Dysplastically in Viva.
844 97. Deng, H., Hillpot, E., Yeboah, P., Mondal, S. & Woodworth, C. D. Susceptibility of
845 epithelial cells cultured from different regions of human cervix to HPV16-induced
846 immortalization. *PLOS ONE* **13**, e0199761 (2018).
847 98. Moody, C. A. & Laimins, L. A. Human Papillomaviruses Activate the ATM DNA
848 Damage Pathway for Viral Genome Amplification upon Differentiation. *PLOS*
849 *Pathog.* **5**, e1000605 (2009).
850 99. Gautam, D. & Moody, C. A. Impact of the DNA Damage Response on Human
851 Papillomavirus Chromatin. *PLOS Pathog.* **12**, e1005613 (2016).
852 100. Anacker, D. C. & Moody, C. A. Modulation of the DNA damage response during
853 the life cycle of human papillomaviruses. *Virus Res.* **231**, 41–49 (2017).
854 101. Moody, C. A. Mechanisms by which HPV Induces a Replication Competent
855 Environment in Differentiating Keratinocytes. *Viruses* **9**, 261 (2017).
856 102. Mac, M. & Moody, C. A. Epigenetic Regulation of the Human Papillomavirus Life
857 Cycle. *Pathogens* **9**, 483 (2020).
858 103. Prati, B., Marangoni, B. & Boccardo, E. Human papillomavirus and genome
859 instability: from productive infection to cancer. *Clinics* **73**, e539s (2018).

860 104. McBride, A. A. & Warburton, A. The role of integration in oncogenic progression
861 of HPV-associated cancers. *PLoS Pathog.* **13**, e1006211 (2017).
862 105. Knipe, D. M. *et al.* Snapshots: chromatin control of viral infection. *Virology* **435**,
863 141–56 (2013).
864 106. Sakakibara, N., Mitra, R. & McBride, A. a. The papillomavirus E1 helicase
865 activates a cellular DNA damage response in viral replication foci. *J. Virol.* **85**,
866 8981–95 (2011).
867 107. Ouyang, C., Lu, G., He, W., Bay, B.-H. & Shen, H.-M. Post-translational
868 Modification in Control of SIRT1 Stability during DNA Damage Response. *Int. J.*
869 *Biol. Sci.* **18**, 2655–2669 (2022).
870 108. Flick, F. & Lüscher, B. Regulation of Sirtuin Function by Posttranslational
871 Modifications. *Front. Pharmacol.* **3**, 29 (2012).
872 109. Yi, J. & Luo, J. SIRT1 and p53, effect on cancer, senescence and beyond. *Biochim.*
873 *Biophys. Acta* **1804**, 1684–1689 (2010).
874 110. Lee, Y.-H., Kim, S.-J. & Surh, Y.-J. Role of Post-translational Modification of
875 Silent Mating Type Information Regulator 2 Homolog 1 in Cancer and Other
876 Disorders. *J. Cancer Prev.* **27**, 157–169 (2022).
877 111. Chung, S.-H. & Lambert, P. F. Prevention and treatment of cervical cancer in mice
878 using estrogen receptor antagonists. *Proc. Natl. Acad. Sci. U. S. A.* **106**, 19467–
879 19472 (2009).
880 112. Shultz, L. D. *et al.* Human Lymphoid and Myeloid Cell Development in NOD/LtSz-
881 scid IL2Rγnull Mice Engrafted with Mobilized Human Hemopoietic Stem Cells 12.
882 *J. Immunol.* **174**, 6477–6489 (2005).

113. Saulters, E. L. *et al.* Differential Regulation of the STING Pathway in Human Papillomavirus-Positive and -Negative Head and Neck Cancers. *Cancer Res. Commun.* **4**, 118–133 (2024).

114. Smola, H. *et al.* Dynamics of Basement Membrane Formation by Keratinocyte–Fibroblast Interactions in Organotypic Skin Culture. *Exp. Cell Res.* **239**, 399–410 (1998).

115. Bristol, M. L. *et al.* DNA Damage Reduces the Quality, but Not the Quantity of Human Papillomavirus 16 E1 and E2 DNA Replication. *Viruses* **8**, 175 (2016).

116. James, C. D. *et al.* Human Papillomavirus 16 E6 and E7 Synergistically Repress Innate Immune Gene Transcription. *mSphere* **5**, e00828-19 (2020).

117. James, C. D. *et al.* Restoring the DREAM Complex Inhibits the Proliferation of High-Risk HPV Positive Human Cells. *Cancers* **13**, 489 (2021).

118. James, C. D. *et al.* SAMHD1 Regulates Human Papillomavirus 16-Induced Cell Proliferation and Viral Replication during Differentiation of Keratinocytes. *mSphere* **4**, e00448-19 (2019).

119. Gauson, E. J. *et al.* Failure to interact with Brd4 alters the ability of HPV16 E2 to regulate host genome expression and cellular movement. *Virus Res.* **211**, 1–8 (2016).

120. Gauson, E. J. *et al.* Regulation of human genome expression and RNA splicing by human papillomavirus 16 E2 protein. *Virology* **468–470**, 10–18 (2014).

121. Fontan, C. T. *et al.* A Critical Role for p53 during the HPV16 Life Cycle. *Microbiol. Spectr.* **10**, e0068122 (2022).

905 122. Prabhakar, A. T. *et al.* Human Papillomavirus 16 E2 Interaction with TopBP1 Is
906 Required for E2 and Viral Genome Stability during the Viral Life Cycle. *J. Virol.*
907 **97**, e00063-23 (2023).
908 123. Bajikar, S. S. *et al.* Tumor-Suppressor Inactivation of GDF11 Occurs by Precursor
909 Sequestration in Triple-Negative Breast Cancer. *Dev. Cell* **43**, 418-435.e13 (2017).
910 124. Nagatani, M. *et al.* Comparison of biological features between severely immuno-
911 deficient NOD/Shi-*scid Il2rg*^{null} and NOD/LtSz-*scid Il2rg*^{null} mice. *Exp. Anim.* **68**,
912 471–482 (2019).
913 125. Sannigrahi, M. K. *et al.* HPV E6 regulates therapy responses in oropharyngeal
914 cancer by repressing the PGC-1α/ERRα axis. *JCI Insight* **7**, e159600.
915 126. Turk, A. N., Byer, S. J., Zinn, K. R. & Carroll, S. L. Orthotopic xenografting of
916 human luciferase-tagged malignant peripheral nerve sheath tumor cells for in vivo
917 testing of candidate therapeutic agents. *J. Vis. Exp. JoVE* 2558 (2011)
918 doi:10.3791/2558.
919 127. DeRose, Y. S. *et al.* Patient-derived models of human breast cancer: protocols for in
920 vitro and in vivo applications in tumor biology and translational medicine. *Curr.*
921 *Protoc. Pharmacol.* **Chapter 14**, Unit14.23 (2013).
922 128. Guillen, K. P. *et al.* A breast cancer patient-derived xenograft and organoid platform
923 for drug discovery and precision oncology. 2021.02.28.433268 Preprint at
924 https://doi.org/10.1101/2021.02.28.433268 (2021).
925 129. Animal Procedures and Information | Lab Manual and Procedures | Wicha Lab.
926 https://www.med.umich.edu/wicha-lab/labmanual6.html.

130. Whitfield, J., Littlewood, T. & Soucek, L. Tamoxifen Administration to Mice. *Cold Spring Harb. Protoc.* **2015**, 269–271 (2015).

131. Caneparo, C., Baratange, C., Chabaud, S. & Bolduc, S. Conditioned medium produced by fibroblasts cultured in low oxygen pressure allows the formation of highly structured capillary-like networks in fibrin gels. *Sci. Rep.* **10**, 9291 (2020).

132. Ghani, N. 'Izzah A. *et al.* Effect of Different Collection Times of Dermal Fibroblast Conditioned Medium (DFCM) on In Vitro Re-Epithelialisation Process. *Biomedicines* **10**, (2022).

133. Halbert, C. L., Demers, G. W. & Galloway, D. A. The E7 gene of human papillomavirus type 16 is sufficient for immortalization of human epithelial cells. *J. Virol.* **65**, 473–478 (1991).

Figure Legends Figure

Figure 1: Estrogen fails to sensitize *in vivo*.

1A. HeLa cells are an integrated HPV18+ female cervical cancer cell line, we therefore chose to utilize female NOD-scid IL2Rgnull (NSG) mice for this treatment paradigm; we did not choose to ovariectomize these mice. Day 0 marks the date at which cells were injected for xenografts. Tumors were palpable on day 10, mice were randomized. Estrogen alone (E=0.4mg pellet + 8 µg/ml water supplementation *ad libitum*), radiation alone (IR=10 Gy), as well as the combinational approach (E+IR) were monitored for effects on tumor volume by calipers. 1B. Mice were monitored for weight throughout the study. 1C. UMSCC104 cells are an episomal HPV16+ male oropharyngeal line, we

951 therefore chose to utilize male NSG mice for this treatment paradigm. Day 0 marks the
952 date at which cells were injected for xenografts; early estrogen water supplementation
953 began on this day, pellets were later added when tumors were palpable (8 µg/ml water
954 supplementation *ad libitum*). Tumors were palpable on day 7. Estrogen alone (0.4mg
955 pellet + 8 µg/ml water supplementation ad libitum), radiation alone (5 Gy), as well as the
956 combinational approach were monitored for effects on tumor volume by calipers. 1D.
957 Mice were monitored for weight throughout the study.
958
959 **Figure 2: Fibroblasts significantly reduce HPV-specific estrogenic sensitization in**
960 **keratinocytes.** (A) N/Tert-1, (B) HFK+E6E7, and (C) HFK+HPV16 cells were seeded
961 on day 0 and grown in the presence or absence of J2s that had been seeded at least 6
962 hours prior. Cells were washed to remove J2s in noted conditions, trypsinized, and
963 counted on day 3. *, $p < 0.05$; ***, $p < 0.001$.
964
965 **Figure 3: Fibroblasts significantly reduce HPV-specific cancer estrogenic**
966 **sensitization.** J2s were seeded in the morning and noted nuclear-labeled cancer cells
967 were seeded at least 6 hours after: HeLa (A,B), UMSCC47 (C,D), UMSCC104 (E,F),
968 HN30 (G,H). Co-culture images for quantitation were taken the following morning and
969 are set at day 0, estrogen (E) was added immediately after initial imaging on day 0. Cells
970 were again imaged at day 1 and day 3. UMSCC104 cells were grown for an additional
971 time point; these were replenished with new J2s and estrogen on day 3 (post-imaging)
972 and day 5 and imaged again on day 7. Within same graphs *$p<0.05$, ***$p<0.001$. J2s
973 altered growth rates for some of the cell lines and graphs are presented as separate for

974 visual simplicity, but experiments were run concurrently; comparing top and bottom
975 graphs $p<0.05 J2 increased growth, &p<0.05 J2 decreased growth.
976
977 **Figure 4: Human fibroblasts (HDFM) significantly reduce HPV-specific cancer**
978 **estrogenic sensitization.** HeLa were seeded into standard media (A), J2 conditioned
979 media (B), or HDFMs were seeded in the morning and nuclear-labeled HeLa cells were
980 seeded at least 6 hours after (C). Co-culture images for quantitation were taken the
981 following morning and are set at day 0, estrogen (E) was added immediately after initial
982 imaging on day 0. Cells were again imaged at day 1 and day 3. *p<0.05
983
984 **Figure 5: Fibroblasts do not alter cisplatin sensitivity.** J2s were seeded in the morning
985 and noted nuclear-labeled cancer cells were seeded at least 6 hours after: HeLa (A,B),
986 UMSCC47 (C,D), UMSCC104 (E,F), HN30 (G,H). Co-culture images for quantitation
987 were taken the following morning and are set at day 0, noted concentrations of cisplatin
988 were added immediately after initial imaging on day 0. Cells were again imaged at day 1
989 and day 2. New J2s or media were replenished on day 3, and imaged again on day
990 5. Within same graphs ****p<0.001. J2s altered growth rates for some of the cell lines
991 and graphs are presented as separate for visual simplicity, but experiments were run
992 concurrently; comparing top and bottom graphs $$p$<0.05 J2 increased growth, &p<0.05
993 J2 decreased growth.
994
995 **Figure 6: Stroma supports transcriptional regulation, viral protein expression, and**
996 **episomal maintenance; estrogenic transcriptional regulation is lost with stroma.** (A)

997 N/Tert-1 cells were transfected with 1 μg of pgl3 basic backbone, 1 μg of pgl3 control
998 (positive control), or 1 μg LCR and grown in the presence or absence of 15 μM estrogen
999 and/or J2s that had previously been seeded. Forty-eight hours after transfection, a
1000 luciferase-based assay was utilized to monitor levels of LCR transcription. Data are
1001 presented as relative fluorescence units (RFU), normalized to total protein concentration
1002 as monitored by a standard bovine serum albumin (BSA) assay. ANOVA **, $P < 0.01$;
1003 ***, $P < 0.001$ (B) N/Tert-1 cells were grown in the presence or absence of J2s. Cells
1004 were washed to remove J2, then lysed and analyzed via western blotting for ERα.
1005 GAPDH was used as a loading control. (C) HFK^{+}HPV16 cells were seeded on day 0 and
1006 grown in the presence or absence of J2s for 1 week. Cells were washed to removed J2,
1007 then lysed and analyzed for DNA expression of E2 and E6 via the exonuclease V assay,
1008 in comparison to GAPDH and mitochondrial DNA controls. Results are presented as
1009 percent integration as calculated from the cut ratio of matched GAPDH. *$P < 0.05$. (D)
1010 HFK+E6E7 (lanes 2,3) and HFK^{+}HPV16 (lanes 4,5) and N/Tert-1 (lanes 6,7) cells were
1011 seeded on day 0 and grown in the presence or absence of J2s for 1 week. Lane 1 is an
1012 input lysate from J2 alone to control for any background level of expression in fibroblasts
1013 that were not removed via washing. Cells were washed to remove J2s in noted conditions,
1014 trypsinized, lysed, and analyzed via western blotting for SIRT1, pRb, p53, γH2aX, and
1015 E7. GAPDH and β-actin were utilized as loading controls.
1016
1017 **Figure 7: Fibroblast co-culture demonstrates SERMs are worth assessing in an**
1018 **HPV+ *in vivo* model.** J2s were seeded in the morning and noted nuclear-labeled cancer
1019 cells were seeded at least 6 hours after: HeLa (A,B), UMSCC47 (C,D), UMSCC104

(E,F). Co-culture images for quantitation were taken the following morning and are set at day 0, 10 µg raloxifene (R) or 10 µg tamoxifen (T) were added immediately after initial imaging on day 0. Cells were again imaged at day 1 and day 3. UMSCC104 cells were grown for an additional time point; these were replenished with new J2s and drugs on day 3 (post-imaging) and day 5 and imaged again on day 7. Within same graphs *p<0.05, ***p<0.001. J2s altered growth rates for some of the cell lines and graphs are presented as separate for visual simplicity, but experiments were run concurrently.

Figure 8: Fibroblast *in vitro* co-culture SERM assessment in UMSCC104 cells predicted the utility *in vivo*. As described in Figure 1, UMSCC104 cells were injected for xenografts in male NOD-scid IL2Rgnull (NSG) mice. Day 0 marks the date at which cells were injected for xenografts. (A,B) Tumors were palpable on day 7. 1-Control, 2-Raloxifene alone (1.5 mg), 3-Tamoxifen alone (1.0 mg), 4-radiation alone (4 Gy) (IR), as well as the combinational approaches (5-Raloxifene+IR, 6-Tamoxifen+IR) were monitored for effects on tumor volume by calipers. These experiments were run concurrently but presented on separate graphs for visual clarity (groups have been numbered for this clarity). Data points shown for Mean Tumor Volume are representative of conditions with at least 70% of animals remaining. (C) Kaplan-Meier Survival plots the survival curve of the animals treated. This data includes any mice that needed to be sacrificed due to tumor ulceration. (D) Mice were monitored for weight throughout the study. *p<0.05, **p<0.01 ***p<0.001 from control, $p<0.05 from IR alone, colors of * or $ are matched to colors of corresponding conditions that are significant from control or radiation alone, respectively.

Figure 9. Representative cell culture images quantified via Keyence. Images presented are day 5 of UMSCC104 cell cultures in the presence or absence of J2s. Images were captured at 10x in brightfield and TexasRed. All cell lines at all time points were counted utilizing the same control-established automated parameters to ensure reproducibility.

A.

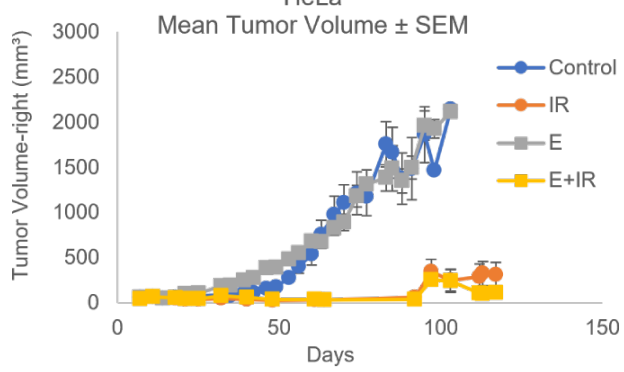

B.

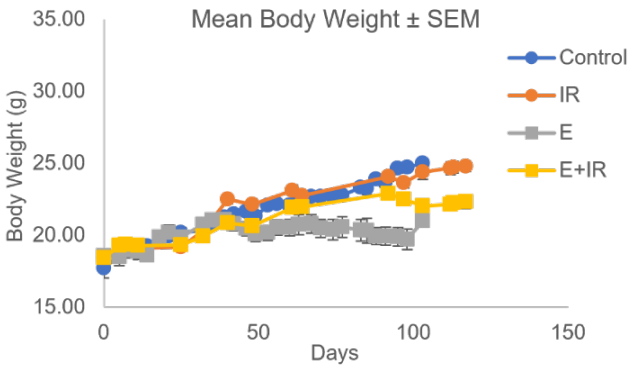

C.

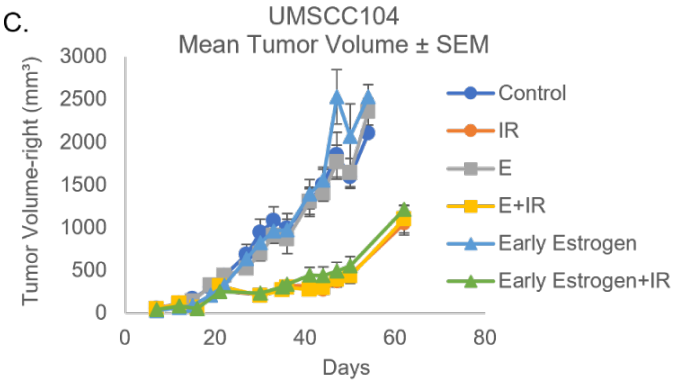

D.

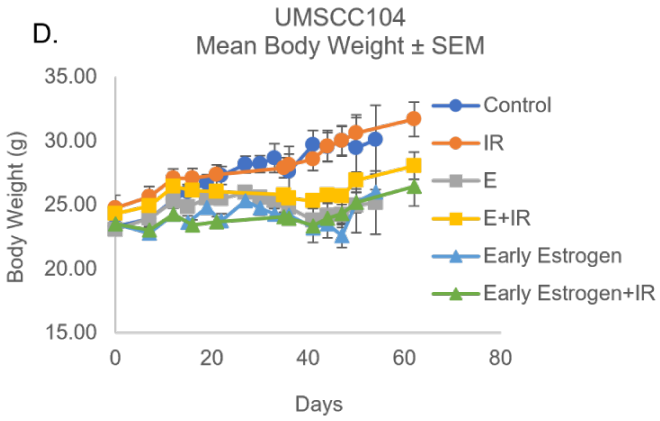

A.

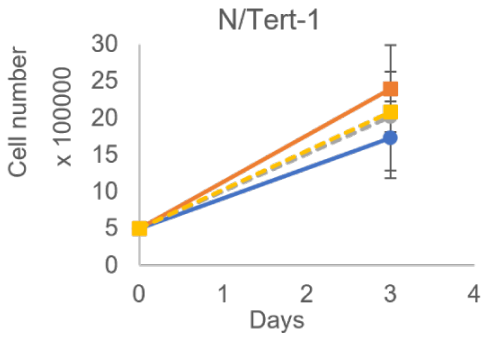

B.

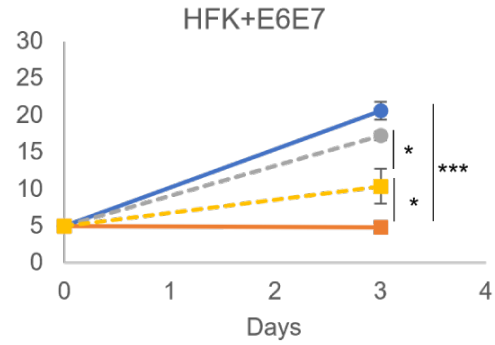

C.

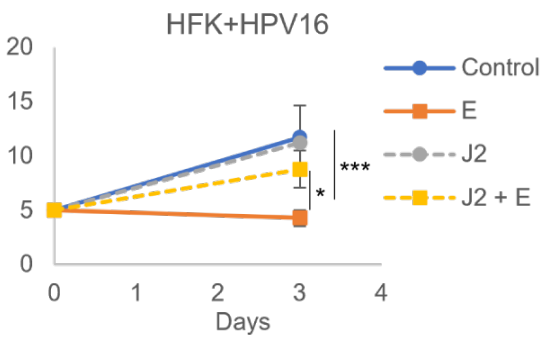

A.

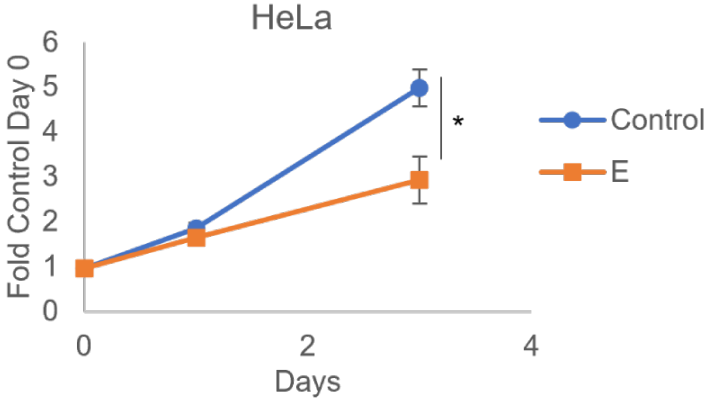

B.

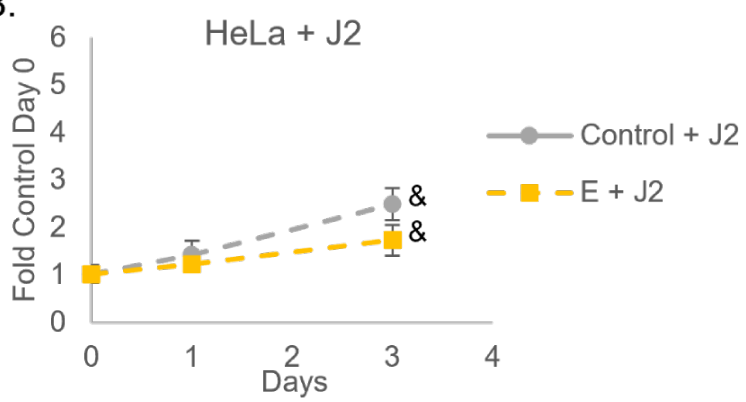

C.

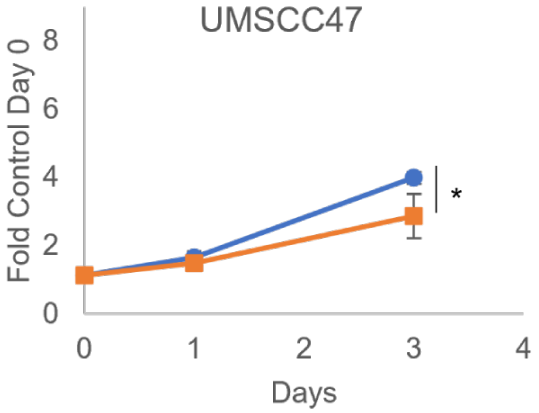

D.

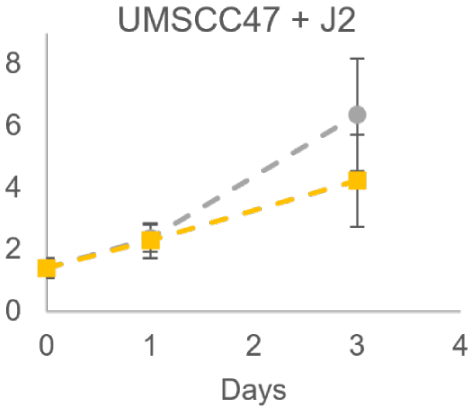

E.

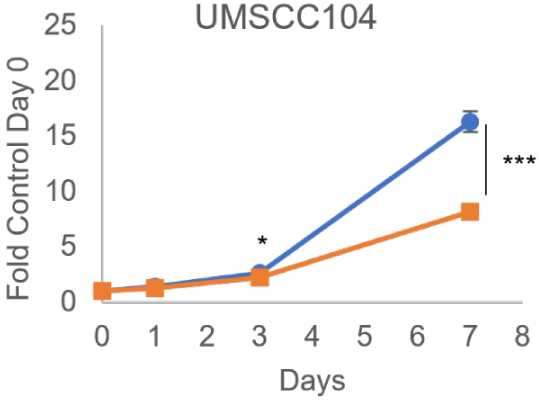

F.

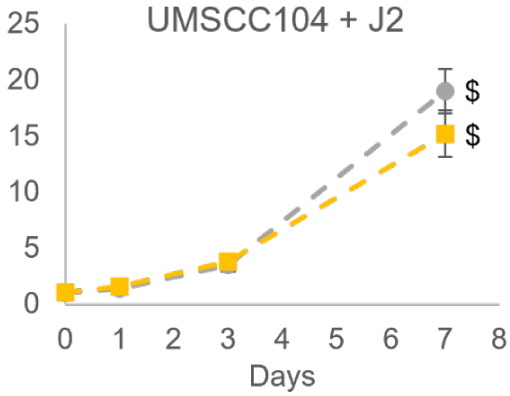

G.

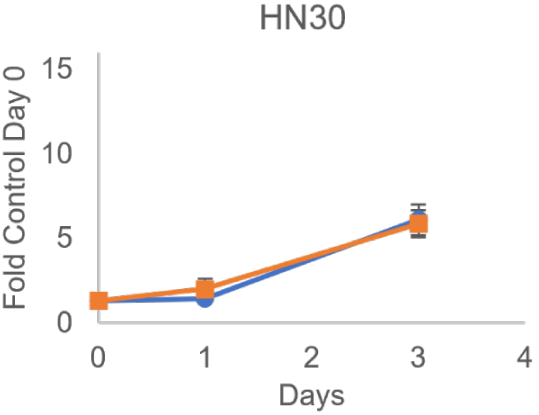

H.

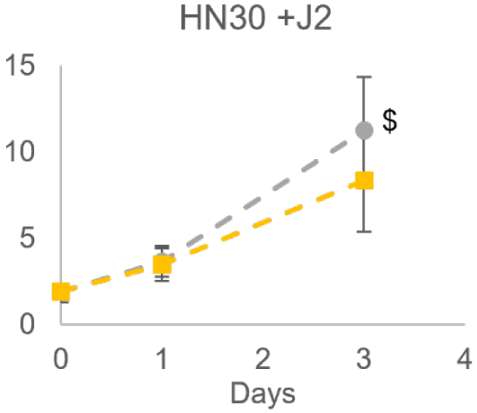

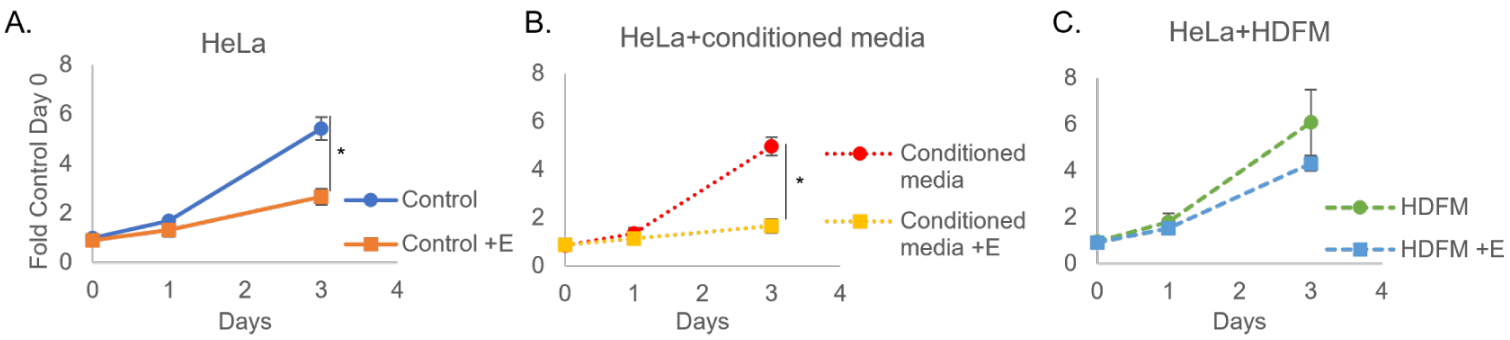

A.

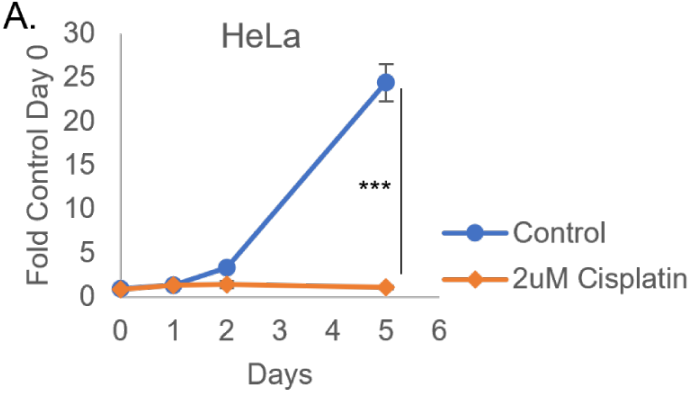

B.

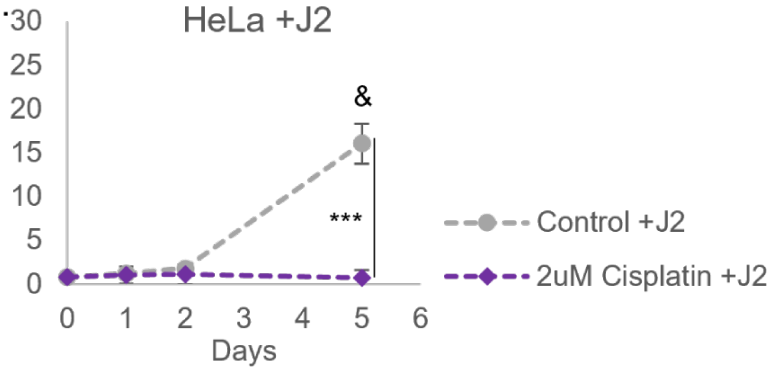

C.

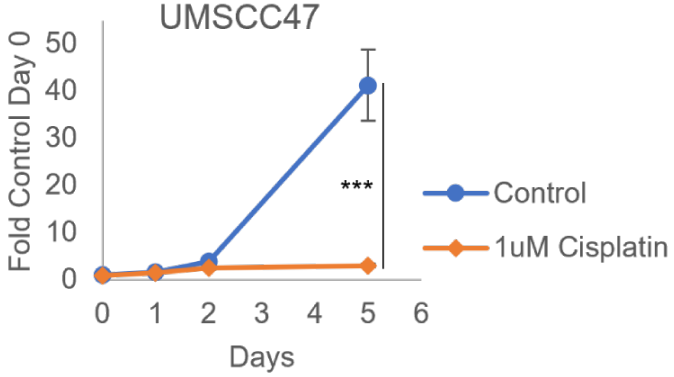

D.

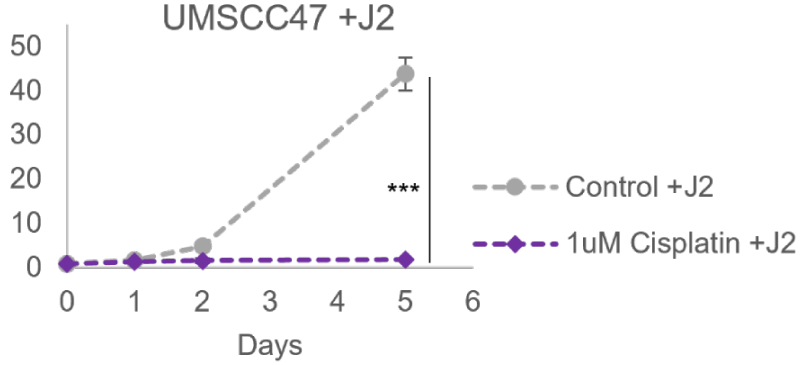

E.

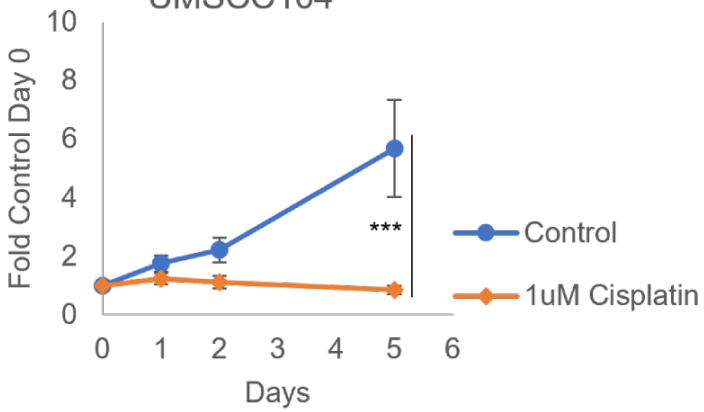

F.

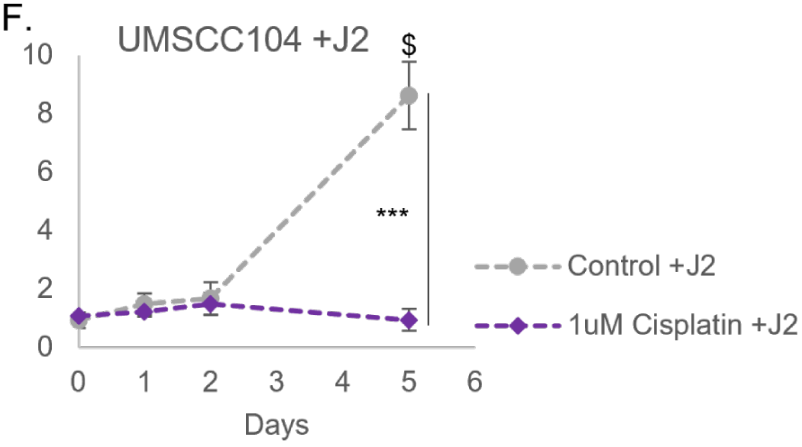

G.

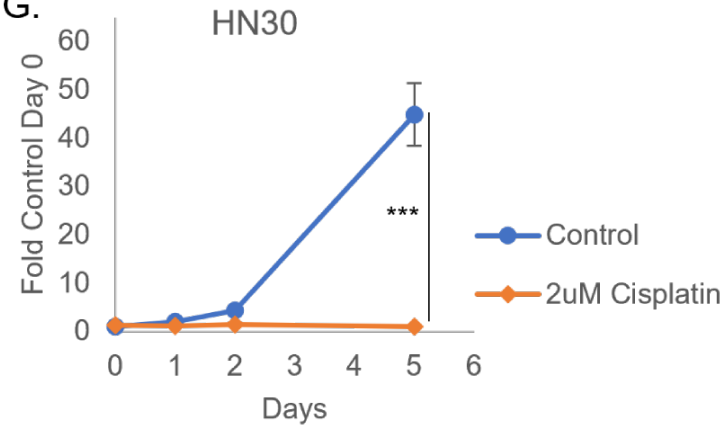

H.

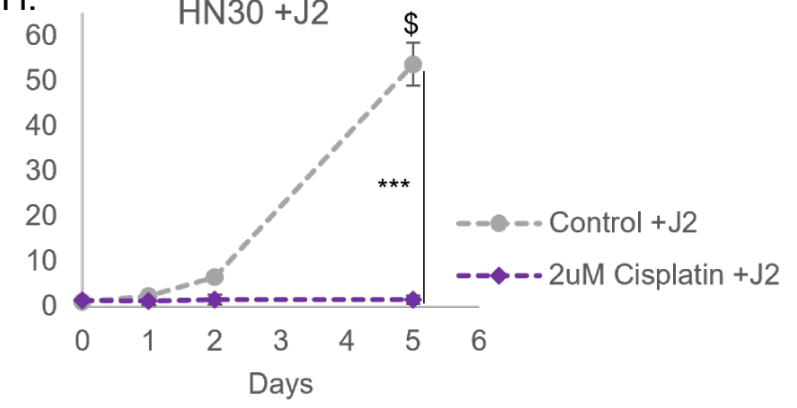

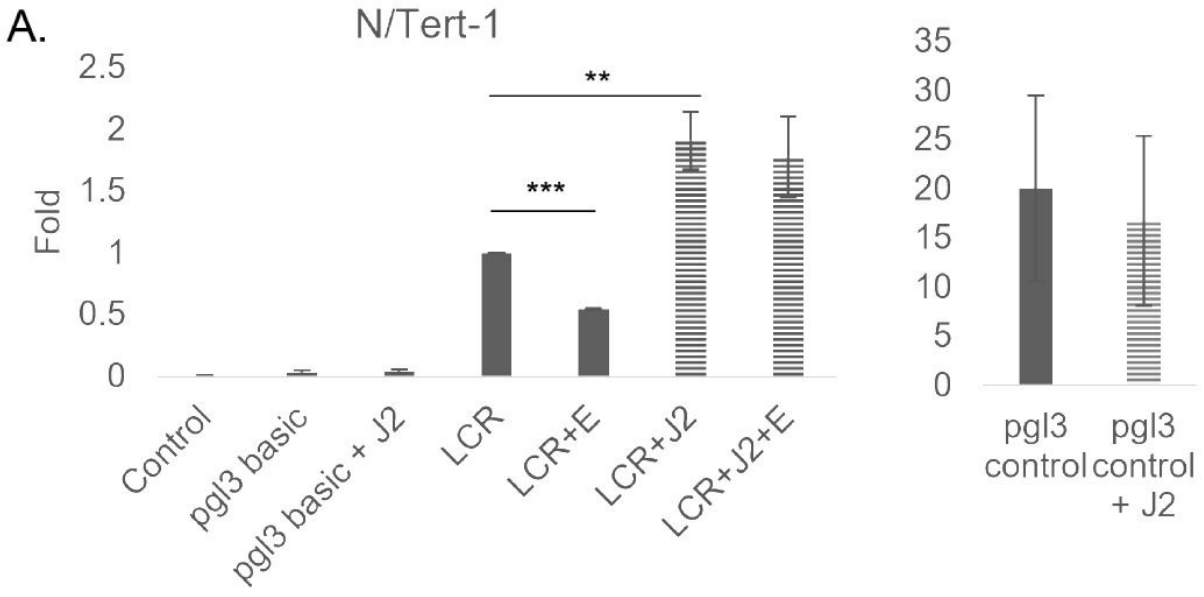

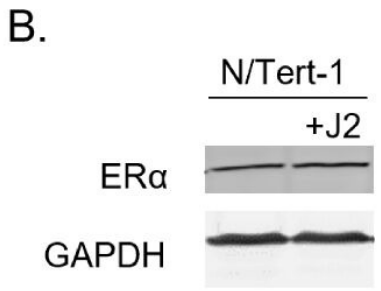

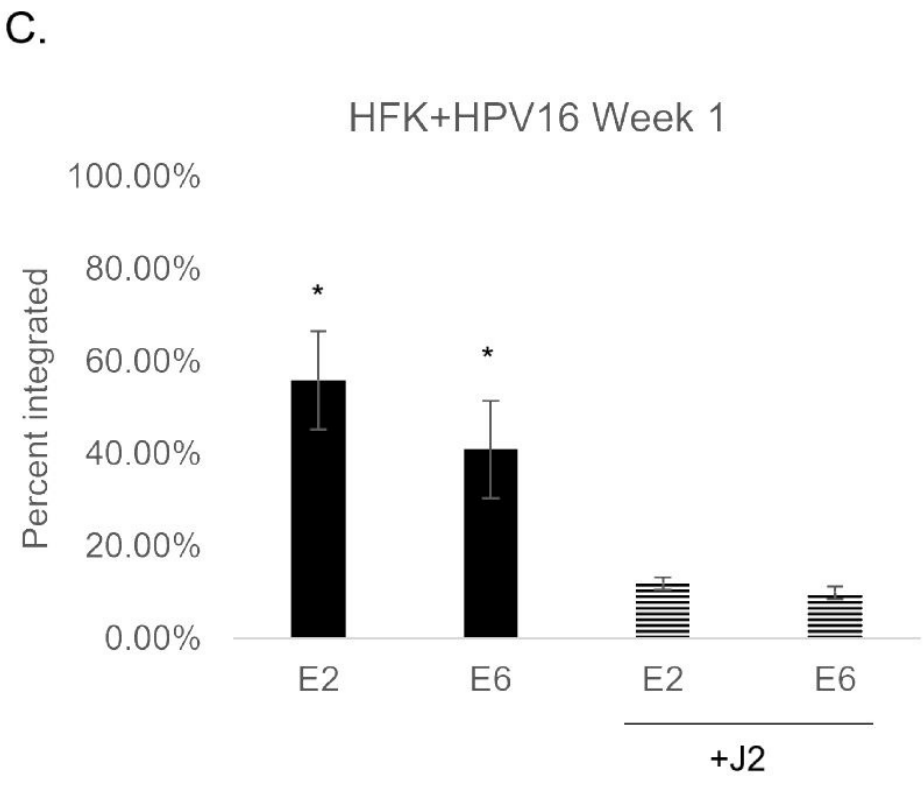

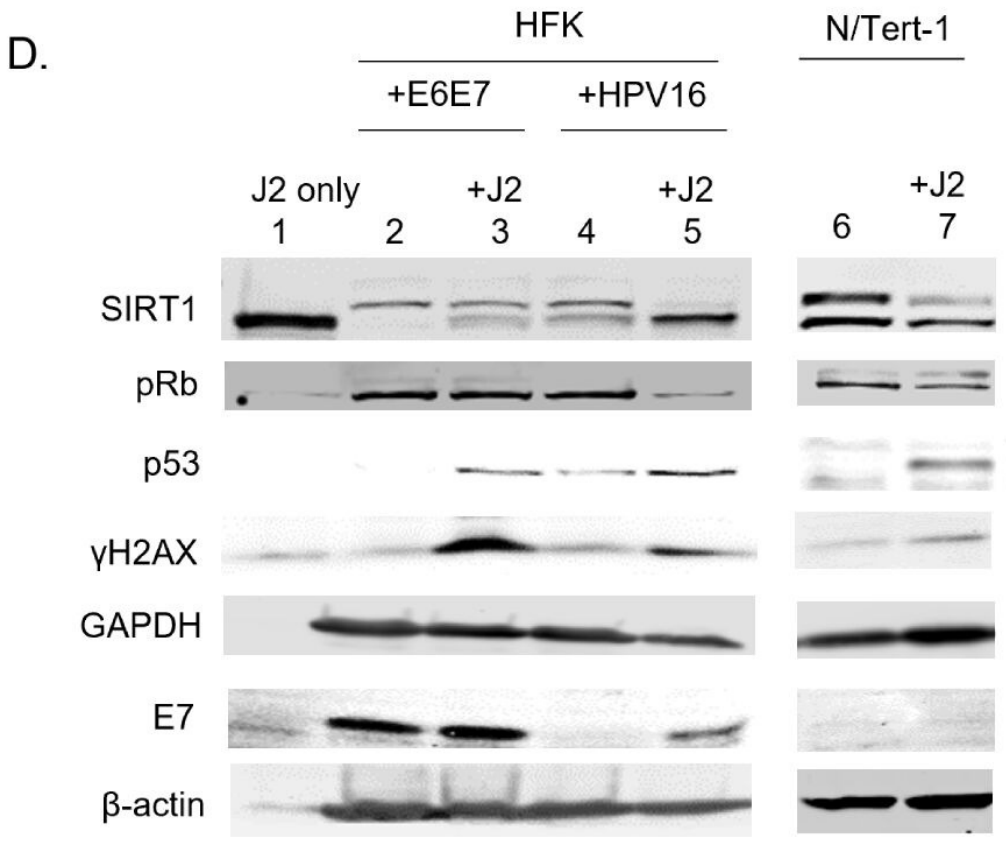

A.

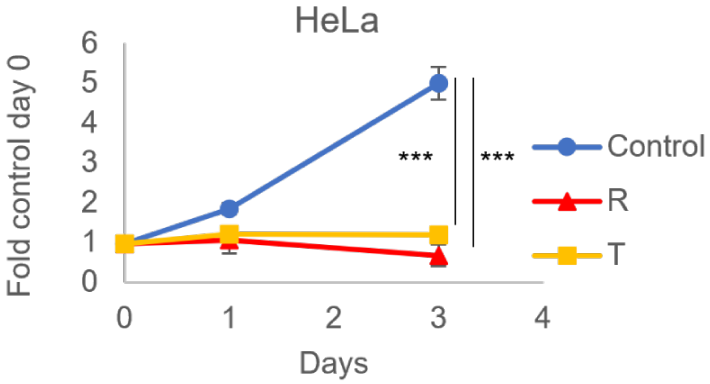

B.

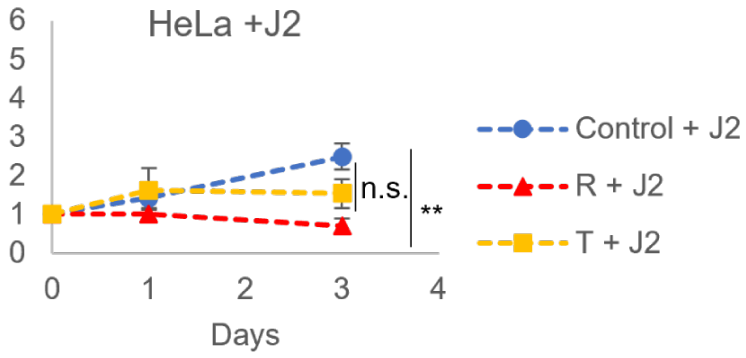

C.

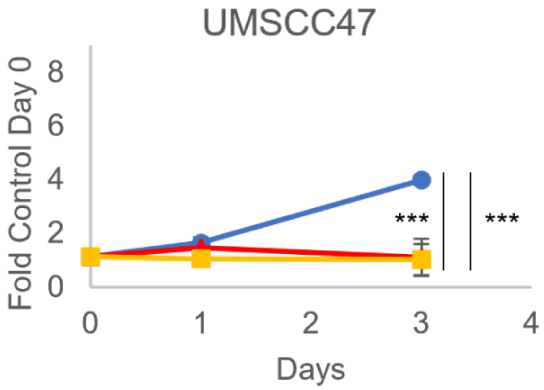

D.

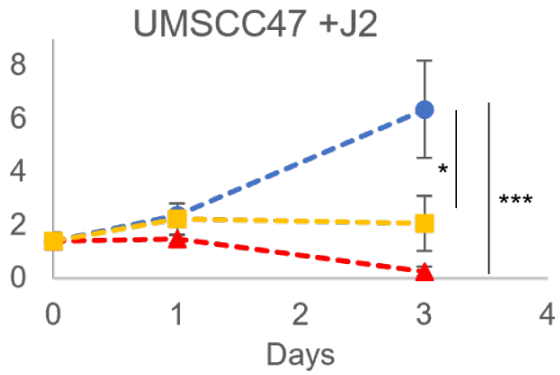

E.

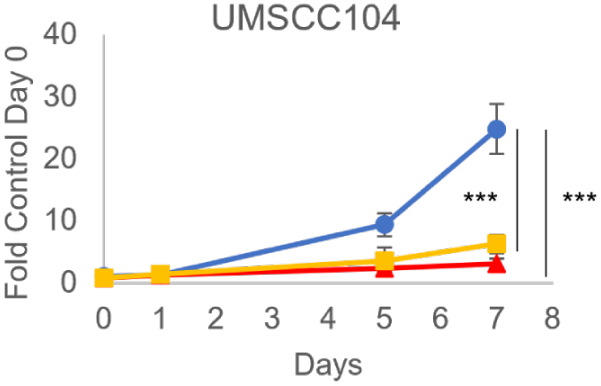

F.

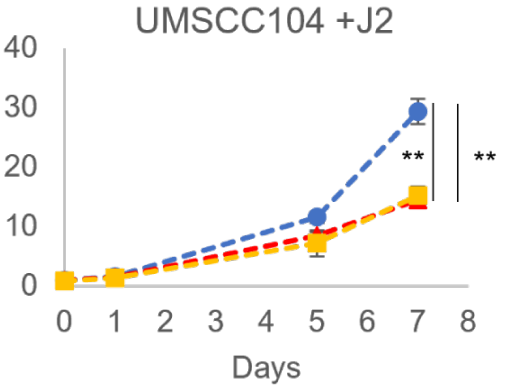

A.

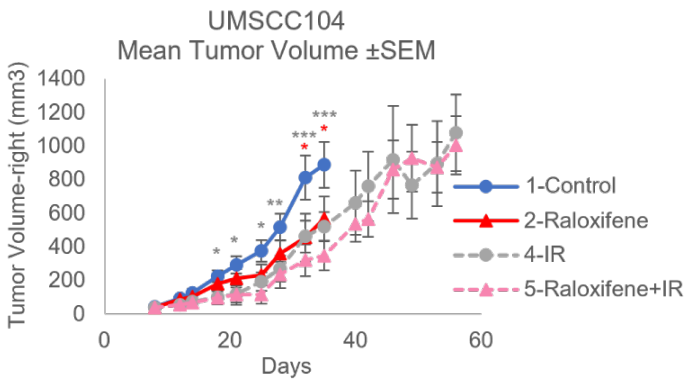

B.

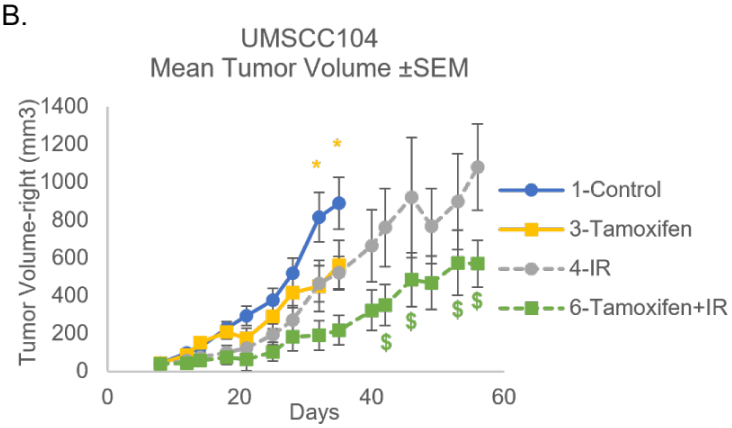

C.

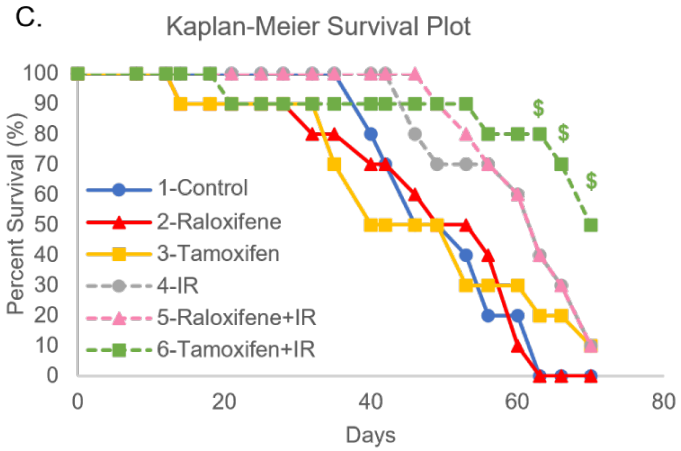

D.